Maximizing Driving Range for Fuel Cell Range Extender Vehicles with Fixed Energy Storage Costs

Maximizing Driving Range for Fuel Cell Range Extender Vehicles with Fixed Energy Storage Costs

by

Jingting Dong

A thesis

presented to McMaster University

in partial fulfillment

of the requirements for the degree of

Masters of Applied Science

in Electrical and Computer Engineering

Hamilton, Ontario, Canada, 2022

Descriptive Note

Masters of Applied Science (2022)	McMaster University
Electrical and Computer Engineering	Hamilton, Ontario

Title: Maximizing Driving Range for Fuel Cell Range Extender Vehicles with Fixed Energy Storage Costs

Author: Jingting Dong, B. Eng. (Hohai University)

Supervisor: Dr. Jennifer Bauman, P. Eng.

Number of Pages: 80

Acknowledgments

I would like to express my deepest gratitude to my supervisor Dr. Bauman for her invaluable support in my graduate studies. She has been consistently giving me positive feedback and advice in my research, this thesis would not have been accomplished without her guidance. I am also so grateful for her patience and wisdom in my personal life during the three years of study, which is helpful to motivate me in my research and career path. Thank you for accepting me as your student and saving me from tedious old work life, I am lucky to be part of your team.

I also would like to express my appreciation to my friends and lab mates, they have given me great help in my school life, especially during the pandemic. Many thanks to Alice and Henry for helping me with my courses study and thesis. Thanks to Ming and Han for being my academic and emotional support. Thank you to Mike who is the inspiration for me to get into auto industry, I would not be here and achieve this accomplishment without his continuous encouragement. Thanks for always believing in me and letting me be myself.

Last but not the least, I will be forever grateful to my mother who has always been supporting me on all decisions I have made. Thanks for letting me to pursue my life.

Abstract

Industry and researchers are investigating both battery electric vehicles (BEVs) and fuel cell hybrid vehicles (FCHV) for the future of sustainable passenger vehicle technology. While BEVs have clear efficiency advantages, FCHVs have key benefits in terms of refueling time and energy density.

This thesis first proposes the concept of a fuel cell range extended vehicle (FCREV) that uses *Whole-Day Driving Prediction* (WDDP) control, which uses driver destination inputs to determine whether the planned driving trips that day will exceed the useable battery energy capacity. If so, the fuel cell is turned on at the start of the day. The benefit of WDDP control is that a smaller, lower cost fuel cell can be used to greatly extend the driving range, since the fuel cell can charge the battery during both driving and parked periods of the day. Furthermore, this research proposes a fast analytical optimization algorithm for designing a WDDP-FCREV to maximize range on a given drive cycle for a set cost. The results show an optimized WDDP-FCREV can greatly exceed the range of a same-cost BEV, by 105% to 150% for no H_2 refueling and by 150% to 250% when H_2 refueling is allowed every 4 hours.

Table of Contents

List of Figures

Chapter 1

Introduction

1.1 Background and Motivations

In the race towards a sustainable electrified transportation system, much debate has focused on the future propulsion system of passenger vehicles: batteries or fuel cells? The main benefits of battery electric vehicles (BEVs) are the higher grid-to-wheels efficiency and the convenience of at-home overnight electric charging. Conversely, a fuel cell hybrid vehicle (FCHV) powered with hydrogen created by electrolysis (using electricity from the grid) can have nearly half the grid-to-wheels efficiency as BEVs, once the electrolyzer [1], compressor [2], and fuel cell [3] losses are considered. The fact that BEVs are nearly twice as efficient as FCHVs supports the position of many automotive manufacturers focused heavily on BEVs, such as Tesla, GM, BYD, and Ford.

However, BEVs have challenges such as limited range, long charge times, and large costly batteries. Since most people drive less than 50 km on an average day [4], a moderate-sized battery with a reasonable cost can provide the required range, and vehicles can conveniently charge with Level 2 charging (up to 19 kW [5]) at home overnight. However, on days when driving needs go far above the average, BEV drivers must carefully consider driving range, find available charging stations, and must either interrupt their trip with long charge times or use fast charging, which can worsen battery health [6] and lower charging efficiency [7]. Driving range can be extended by using very large BEV batteries, but this increases vehicle cost and mass, and midday charging may still be required for very long-distance driving days.

FCHVs offer a zero-tailpipe emission alternative to BEVs, with the advantages of higher energy density, which leads to long driving ranges, and faster refueling times [8].

When hydrogen is compressed to 700 bar, as is common in automotive applications [9], its energy density is 120 MJ/kg [10] compared to 0.9 MJ/kg for a modern automotive lithium-ion battery [11]. With hydrogen refueling times on par with those of gasoline [8], investment in the hydrogen refueling infrastructure remains a critical challenge to widespread FCHV adoption. Automotive manufacturers such as Toyota and Hyundai have focused heavily on polymer electrolyte membrane fuel cells, resulting in the Toyota Mirai and the Hyundai Nexo [12] passenger FCHVs. However, heavy-duty transport trucks are prime candidates for hydrogen-powered fuel cells because their high energy needs and demanding drive cycles are well satisfied by the high energy density, long range, and fast refueling times of hydrogen [13]. Thus, there is increasing interest from manufacturers to develop fuel cell trucks, including Hyundai, who launched the world's first mass-produced fuel cell transport truck, XCIENT, in 2020 [14], and Nikola Motor, who announced a North American hydrogen fuel cell commercial truck program in March 2021 [15].

To support the increase of fuel cell heavy-duty transport trucks in the coming years, an increase in hydrogen refueling stations is crucial [16], [17], ideally using hydrogen created by electrolysis using renewable energy, since renewable energy sources like wind and solar often require energy storage due to their variable nature [8], [18]. This thesis proposes that the anticipated proliferation of hydrogen stations along highways to support heavy-duty transport can be leveraged as well for the passenger vehicle segment, which is the focus of this thesis. By adding a relatively small range-extending fuel cell to a passenger BEV, which is the fuel cell range extender vehicles (FCREVs), drivers can easily make use of these highway hydrogen stations on long-distance driving days, while continuing to use convenient at-home overnight charging on average driving days.

Determination of a long-distance driving day can be made using the driver's planned destinations for the day input into the vehicle navigation system. Using standard navigational maps, the planned distance can be calculated, and historical vehicle energy consumption can be multiplied by the planned distance to get an approximate energy requirement for the day, which is then compared to the available energy in the battery at the start of the day (usually fully charged overnight). This estimate can be improved if connected traffic data is available, indicating the speed limits for each road segment, which can be used to refine the estimated vehicle energy consumption. This energy estimate is practically achievable with today's standard navigation and on-board computing systems, as opposed to the precise second-by-second drive cycles required for some optimization-based control strategies.

1.2 Contributions

This thesis proposes a unique control strategy and an optimization algorithm for a passenger FCREV that combines the best features of BEVs (high grid-to-wheels efficiency and convenient at-home charging for most driving days) and FCHVs (longer range and fast refueling times), but without the need for extensive hydrogen fueling infrastructure within cities.

The first contribution of this research is the proposal of a new simple and elegant paradigm for FCREVs using Whole-Day-Driving Prediction (WDDP) control with the consideration of parked times. In this control strategy where on long-distance driving days, the fuel cell should be turned on at the *start* of the driving day, and remain running during parked times to charge the battery. This is possible from a safety standpoint because of the zero harmful tailpipe emissions from fuel cells, in contrast to internal combustion engine range extenders. By allowing the fuel cell much more time to provide energy in the day, the fuel cell size can be decreased, lowering the cost of the vehicle, and making it cost-comparable to a long-range BEV. On a long-distance driving day, the small fuel cell should provide constant power to extend fuel cell lifetime, and only be turned off temporarily if the battery reaches full SOC. On a normal driving day, the fuel cell stays off all day.

Optimizing the component sizes (battery, fuel cell, and hydrogen tank) of a WDDP-FCREV requires consideration of the full-day drive cycle, and the commonly-used analysis on short standard drive cycles will not suffice because the amount of parked time in between trips will affect the daily driving range. Thus, the second contribution of this thesis is the proposal of an analytical design optimization algorithm which can quickly identify the optimal plant and control parameters of a WDDP-FCREV to maximize range on a given full-day drive cycle for a set component cost. This approach is highly accurate and accelerates the optimization process by 20 thousand times compared to running the full model in Simulink Accelerator mode.

The combination of these two contributions leads to FCREV designs that can achieve significantly longer range compared to a baseline BEV (Chevrolet Bolt) for the same energy storage cost. The cost constraint is a defining feature of the research, which keeps the component sizes to reasonable values in the optimization search. Thus, the thesis contributions have valuable practical implications for the future design of long-range emission-free passenger vehicles.

1.3 Publications

The research for this thesis has resulted in the following publication:

J. Dong and J. Bauman, " Maximizing Driving Range for Fuel Cell Range Extender Vehicles with Fixed Energy Storage Costs," *IEEE Trans. on Transportation Electrification*, accepted in August 2022.

1.4 Outline of the Thesis

This thesis is organized into six chapters. Chapter 1 has given a comparison between BEVs and FCHVs, as well as motivation for FCREVs. Chapter 2 reviews the current research on control strategies for FCHVs and FCREVs, especially the advantage of WDDP control strategy applied to FCREVs.

Chapter 3 introduces general design considerations of WDDP-FCREVs, including the proposed WDDP-FCREV control flow, fuel cell lifetime and other important component parameters. Chapter 3 also describes detailed vehicle modeling of the BEV and WDDP-FCREV created in MATLAB/Simulink, along with validation of the BEV model to experimental logged data.

Chapter 4 presents the proposed design optimization algorithm and compares the algorithm-calculated range results to those of the full vehicle model, to validate that the approximations have only a minor impact on the accuracy of the results.

Chapter 5 demonstrates the detailed optimization results from implementing the algorithm on a WDDP-FCREV with various case studies. This chapter presents the range results with optimal component sizing combination on both customized drive cycle and real-world drive cycles. In addition, it also provides optimization results regarding to cost, accessory load and multiple drive cycles. In this chapter, a range comparison to BEV fast-charging with the same refueling/re-charging time is investigated on real-world long drive cycles. Lastly, Chapter 6 gives the summary and suggestions for future work.

Chapter 2

Review of Fuel Cell Range Extender Vehicle Control Strategy

2.1 Control Strategies of FCHVs

The FCHVs that are investigated by most research are powered primarily by hydrogen stored in on-board tanks, with batteries and possibly ultracapacitors used to accept regenerative braking energy and provide high power peaks. The defining feature of FCHVs is that the battery does not plug in to charge from the grid so all traction power ultimately comes from hydrogen. With regards to optimal sizing, [19] proposes an analytical optimization method for designing a fuel cell-battery-ultracapacitor powertrain and [20] uses grey wolf optimization to find optimal sizes of the fuel cell, battery, and ultracapacitor for standard drive cycles. With regards to control of FCHVs, both rule-based [21], [22] and optimization-based [23] – [25] energy management strategies (EMSs) have been proposed. In both cases, common goals are to determine fuel cell, battery, and possibly ultracapacitor power profiles to improve fuel economy and smooth the fuel cell power to extend its lifetime. Fuzzy control algorithms are often proposed for practical implementation of these strategies due to their simplicity and low-computational cost [26] – [28].

2.2 Control Strategies of FCREVs

This thesis focuses on passenger fuel cell range extender vehicles, which have a lager battery that charges from the grid and a smaller fuel cell. Due to the fundamental difference in operation, the process of optimally designing a FCREV is much different than that for a FCHV, and the control strategy has more flexibility due to the larger battery.

Prior research on FCREV control generally assumes fixed battery and fuel cell sizes, and uses either a charge-depleting/charge-sustaining (CD/CS) [29], [30] or blended

[31], [32] EMS. Reference [29] focuses on optimizing the CD/CS EMS for a FCREV with a 16 kWh battery (to achieve 100 km electric range) and a 32 kW fuel cell. Only battery power is used to propel the vehicle until the battery depletes to 30% state-of-charge (SOC) in CD mode, then a genetic algorithm is used to optimally split the fuel cell and battery power in CS mode. However, the genetic algorithm approach requires the precise drive cycle ahead of time and is time-consuming, so is not well-suited to real-time implementation. Similarly, [30] has a 30 kW fuel cell range extender and uses CD/CS control with only the battery providing power until its SOC reaches 30%. For CS mode, [30] proposes a two-stage controller to minimize hydrogen consumption and extend fuel cell lifetime by smoothing fuel cell power. Since rapidly changing fuel cell load may cause fuel starvation, flooding, membrane drying, and pressure imbalance, which can shorten fuel cell lifetime, a steadier fuel cell power and with less on/off switching is recommended to maximize lifetime [30].

With a blended EMS strategy, [31] does not consider electric-only mode, so does not fully explore the possibilities of FCREVs. For a 24.5 kWh battery and 8 kW fuel cell, [31] proposes a nonlinear control strategy with the goal to extend the fuel cell lifetime. The results show that with this smaller fuel cell, it is best to run the fuel cell at constant or near-constant power to improve fuel cell longevity. Reference [32] also proposes a blended strategy, where the goal is to optimally balance fuel cell lifetime and vehicle energy consumption while ensuring the battery SOC reaches its minimum level of 30% at the end of the drive cycle. This study uses a 12.8 kWh battery and a 30 kW fuel cell. Total driving distance is acquired from the navigation system/driver, and then a vehicle speed prediction algorithm is used to predict expected speed based on historical data.

FCREV sizing studies such as [33] and [34] also use the CD/CS control strategy. Reference [33] aims to find the optimal battery and fuel cell sizes on one standard drive cycle using CD mode until the battery reaches 30% SOC. Then, for CS mode, [33] uses Pontryagin's Minimum Principle to solve the global optimization problem of the power split between the fuel cell and battery, where the goal is to minimize hydrogen use. The exact drive cycle must be known ahead of time so this is not a real-time strategy. The component size search space is large (e.g., considering fuel cell sizes from 20 kW to 100 kW), and the resulting optimal sizes (30 kWh battery, > 50 kW fuel cell) are large, indicating a high-cost vehicle. Reference [34] sets the battery size to 29 kWh for a ~50 km electric range of an urban logistics FCREV. The goal is to find the optimal fuel cell size considering energy and component costs. For the typical case of relatively expensive hydrogen, [34] uses the CD/CS strategy (CD mode to 20% SOC), where the CS mode control decisions are made using convex programming, which requires knowledge of the entire drive cycle in advance. Fuel cell sizes of 21 kW – 45 kW are found to be optimal for different drive cycles, though maximum driving range over the day is not considered.

All prior research on FCREV control and sizing considers only the target drive cycle, and does not consider making use of the parked times that occur in between driving times in real-world vehicle usage. Furthermore, most studies use CD/CS control, meaning the battery is mostly depleted before the fuel cell starts providing power. For these two reasons, prior designs must employ relatively large fuel cells to provide enough power over a short period of time so that the added fuel cell energy makes a meaningful impact on the daily range – this increases the vehicle cost.

2.3 Whole-Day Driving Prediction Control Strategy

A similar *Whole-Day Driving Prediction* (WDDP) control concept was proposed by the authors in [35] for application with plug-in hybrid electric vehicles (PHEV) using internal combustion engines. The small engine can be decided if to be turned on based at the start of day trip based on the driver's whole-day trip plan.

However, there are two fundamental differences with now applying WDDP to FCREVs: (i) PHEVs cannot have the engine running while parked due to emissions, so have a smaller window of time to provide power in the day, which changes the component sizing optimization process, and (ii) Range is not a concern for PHEVs since the gas tank can hold a lot of chemical energy and gas stations are ubiquitous, so the focus of [35] was to reduce vehicle cost compared to BEVs. However, the range of FCREVs can be a concern on a long-distance driving day, so the focus of this study is to maximize total range to longer than that of a reference BEV while keeping the vehicle cost equal (or lower).

Chapter 3

FCREVs Using WDDP Control Strategy

3.1 General Design Considerations

The main benefit of using the WDDP control strategy in a FCREV is that since the fuel cell turns on at the start of a long-distance driving day, there will be more time to charge the battery from the fuel cell, and thus more extended range can be obtained from a smaller sized fuel cell, reducing vehicle cost. The proposed WDDP energy management strategy is to turn the fuel cell on at constant power (which is determined in the offline optimization process) at the start of a long-distance driving day – this strategy is simple and easily implementable, and will maximize range, which is a driver's primary concern on long-distance driving days. Fig 3-1 shows the flow diagram of the proposed WDDP-FCREV control, which would run in real-time in the vehicle.

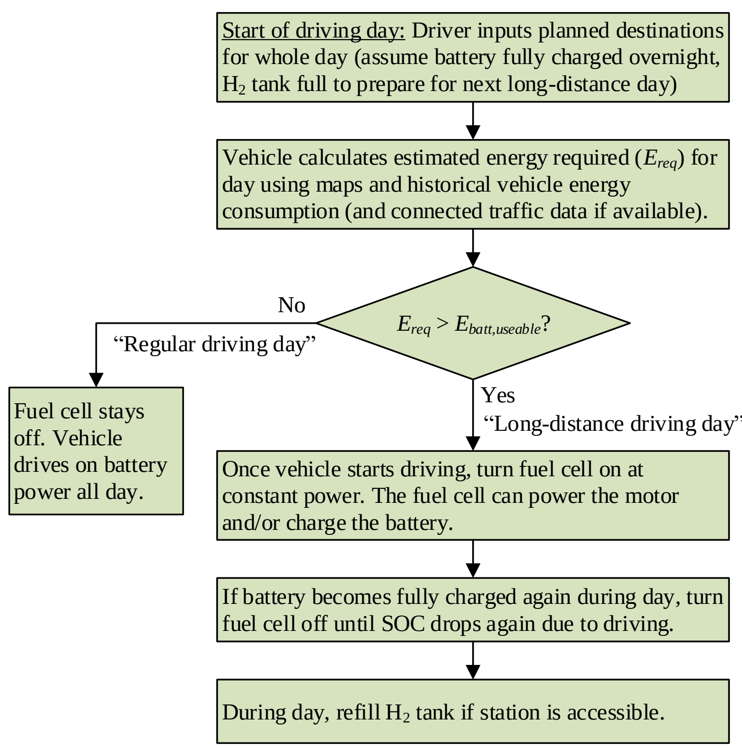

Figure 3- 1: Proposed WDDP-FCREV control flow that runs online in the vehicle

Furthermore, this strategy aligns well with extending fuel cell lifetime compared to a fuel cell in a typical FCHV, which experiences dynamic load changes, frequent start-stop cycles, and idling. Reference [36] performs comprehensive automotive fuel cell lifetime testing and determines that 56% of deterioration occurs due to dynamic load changes, 33% due to start-stop cycling, 6% for high power load, and 5% for idling. While high power loads will occur for both the WDDP-FCREV and the typical FCHV, the other deterioration factors are reduced or eliminated with the proposed WDDP-FCREV since the fuel cell is off most days, runs at a constant power when on, and does not idle. On a long-distance driving day, the fuel cell would only turn off midday (i.e., have an additional start-stop cycle in a day) if the battery SOC reaches its maximum.

While the WDDP-FCREV online control strategy summarized in Fig 3-1 is straightforward and simple to implement in a vehicle, the achievable driving range will depend heavily on the vehicle design stage which occurs offline – this is the focus of the proposed optimization algorithm in this thesis. Fig 3-2 shows the proposed FCREV system diagram, including the most important parameters to optimize in the offline design process: energy capacity of the battery in kWh, E_{batt}, fuel cell rated power in kW, P_{fc}, and mass of hydrogen (H_2) in kg that can be stored in the tank, m_{H2}. A DC/DC boost converter is required after the fuel cell to boost the relatively low voltage of the small fuel cell to that of the high voltage traction battery. Using a smaller fuel cell allows the use of a smaller DC/DC converter, further reducing cost. This research uses cost as the main design constraint, so the total cost of the battery, fuel cell, DC/DC converter, and H_2 tank in the FCREV is fixed, and can be set equal to the battery cost in the compared BEV – then driving range is compared to quantify the FCREV extension over the BEV for the same cost. Thus, there are two degrees of freedom in the component design space: E_{batt} and P_{fc}, since once these are selected, the size of the H_2 tank, m_{H2}, is set based on the cost. There is also one degree of freedom in the control design space: the constant % of rated fuel cell power that the fuel cell operates at when on, R_{fc}.

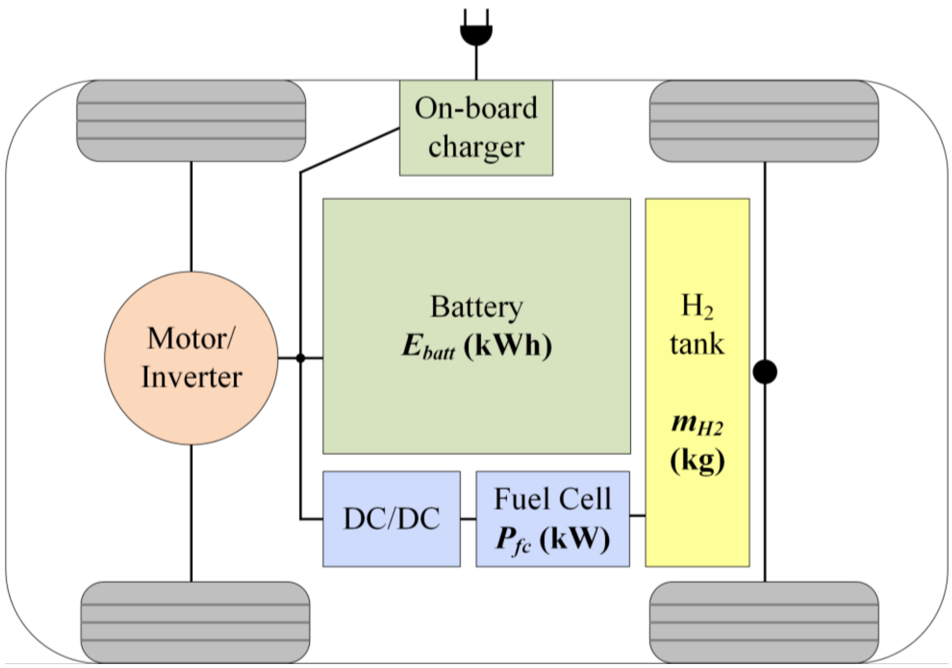

Figure 3- 2: Proposed FCREV system diagram with component design parameters bolded

Though a full Simulink-based vehicle model, as described in the next sections, can be used to analyze these three degrees of design freedom, the simulation time is prohibitively long on long-distance driving cycles to allow a full investigation of the design space. For example, the full vehicle model takes about one minute to run a 700 km full day drive cycle in Accelerator mode for a single component/control specification. If 50 battery sizes are considered with 50 fuel cell sizes and 5 fuel cell rated powers, this equates to 208 hours of simulation time for a single drive cycle. Investigating other drive cycles would multiply this time accordingly. Thus, the proposed analytical optimization algorithm that can be used to investigate the same design space in under 40 seconds. The full Simulink vehicle model described in this section is important to validate the accuracy of the results from the algorithm, as discussed in Chapter 3.

3.2 BEV Vehicle Model and Validation

A Chevrolet Bolt BEV model is created in MATLAB/Simulink according to the vehicle parameters shown in Table 3-1. Fig 3-3 shows a block diagram of the forward-looking BEV model, which at a high level consists of a driver block, controller block, and vehicle plant. The driver block is modeled as a proportional-integral closed loop controller to adjust the vehicle torque request to ensure the vehicle model follows the specified drive cycle. The controller block sends the calculated torque commands to the motor (positive torque for propelling and negative torque for regenerative braking) and wheel (negative torque for friction braking).

The vehicle plant (within the dashed box) is created using standard vehicle modeling equations. Equation (3-1) shows the vehicle speed at the next simulation step, $v_{chas}(t+1)$, is determined by the force out of the wheel block and the aerodynamic losses, where ρ_{air} is the air density (1.23 kg/m^3). The force out of the wheel is calculated by (3-2) using the torque into the wheel (τ_{in_wheel}), the friction braking torque ($\tau_{friction\_brake}$), and the rolling resistance losses, where r_{wheel} is the wheel radius and g is the gravitational constant. The torque into the wheel is calculated by (3-3), where r_{fd} is the final drive ratio and η_{fd} is the final drive efficiency. The battery current is calculated by (3-4) as the sum of the motor current and the electrical accessory current, where η_{motor} is the motor efficiency map based on motor speed and torque (tuned to align with experimentally logged data) and P_{elec_access} includes the power draw for controllers, lights, windshield wipers, heating/air conditioning, etc.

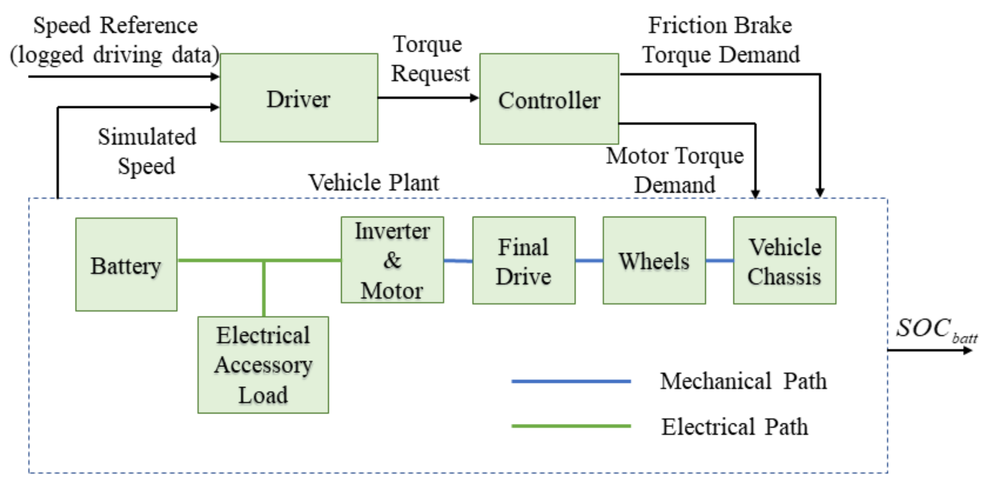

Figure 3- 3: Block diagram of BEV model

TABLE 3-1: Chevrolet Bolt Vehicle Model Parameters

Parameter	Symbol	Value	Reference
Vehicle Mass (kg)	m	1616 + 80 driver	[37]
Drag Coefficient	C_d	0.32	[38]
Rolling Resistance 1	μ_1	0.006	[39]
Rolling Resistance 2	μ_2	0.0001	[39]
Frontal Area (m^2)	A	2.4211	[37]
Tire Size		215/50R17	[37]
Final Drive Ratio	r_{fd}	7.05	[37]
Battery Size (kWh)	E_{batt}	60	[37]

$$v_{chas}(t+1) = v_{chas}(t) + \frac{1}{m}\int_{t}^{t+1}\left(F_{out\_wheel} - \frac{1}{2}\rho_{air}AC_d v_{chas}^2(t)\right)dt \quad \textbf{(3 - 1)}$$

$$F_{out\_wheel} = \frac{\tau_{in\_wheel} + \tau_{friction\_brake}}{r_{wheel}} - (\mu_1 + \mu_2\omega_{wheel})mg \quad \textbf{(3 - 2)}$$

$$\tau_{in\_wheel} = \tau_{motor} r_{fd} \eta_{fd} \quad \textbf{(3 - 3)}$$

$$I_{batt} = \frac{\tau_{motor}\omega_{motor}\eta_{motor} + P_{elec\_access}}{V_{batt}} \quad \textbf{(3 - 4)}$$

The battery model uses the battery current from (3-4) and an initial SOC value to calculate the battery SOC and the battery terminal voltage of the next simulation step, as shown in (3-5) and (3-6). In (3-5), Cap_{batt} is the useable battery capacity in Ah. In (3-6), the battery terminal voltage (V_{batt}) is calculated using either the battery charging or discharging internal resistances (R_{chg}, R_{dischg}) and the open circuit voltage (V_{batt_ocv}), which are all a function of SOC.

$$SOC(t+1) = SOC(t) + \frac{1}{Cap_{batt}}\int_{t}^{t+1}(-I_{batt})dt \quad \textbf{(3 - 5)}$$

$$\begin{aligned} V_{batt} &= V_{batt\_ocv}(SOC) - I_{batt}R_{chg}(SOC) \qquad (when\ I_{batt} < 0) \\ V_{batt} &= V_{batt\_ocv}(SOC) - I_{batt}R_{dischg}(SOC) \quad (when\ I_{batt} \geq 0) \end{aligned} \quad \textbf{(3 - 6)}$$

Four real-world logged drive cycles of the Bolt are used to validate the model. The logged data contains vehicle speed, battery voltage, current, and SOC, air conditioning/heating power, road altitude, and ambient temperature, and is measured with a commercially available CANbus datalogger. The logged air conditioning/heating power is fed into the model on each cycle, since this power use is specific to each trip, as set by the driver. For each drive cycle, the simulated starting SOC is set to the logged SOC at the start of the cycle.

The first step is to create and validate the battery model, since the battery is a critical component of the BEV. The battery model parameters are first estimated/extracted from the experimental data. Fig 3-4 shows these estimated pack parameters as a function of battery SOC. The Chevrolet Bolt has a 60 kWh battery, but only a portion of this represents useable energy, since the battery is never allowed to fully deplete so as to lengthen its lifetime. Analysis of the logged data indicates 89.2% of the energy in the battery is useable, which is about 53.5 kWh. To validate the BEV battery model, the experimentally-logged current is fed into the battery model, and the resulting simulated battery terminal voltage and SOC are compared to the experimental voltage and SOC. Positive battery current represents discharging the battery (propelling the vehicle) and negative battery current represents charging the battery (from regenerative braking). Fig 3-5 shows the experimental current, experimental and simulated voltage, and experimental and simulated SOC for drive cycle #3, which shows excellent agreement between experimental and simulated values, especially considering the simple battery model does not account for temperature effects in the battery (due to lack of data), which are present in the real battery.

Since the ambient temperature was not included as a factor in the battery validation process, there was no temperature data fed into the whole BEV model validation. The average ambient temperatures of the 4 logged drive cycles used for validation are- 2.9 °C, 6.3°C, 20 °C and 9 °C~~[fill in]~~, thus this battery model is calibrated to work well in this range, between 3°C and 20 °C– ~~.~~around. ~~The BEV model is considered to work in a moderate temperature, such as 20°C degree, in this research.~~ Further data would be needed to extend the battery model to work well in very high or very low temperatures. ~~However, it is necessary to consider how the temperature affect battery SOC performance once the experimental data is substantively available.~~

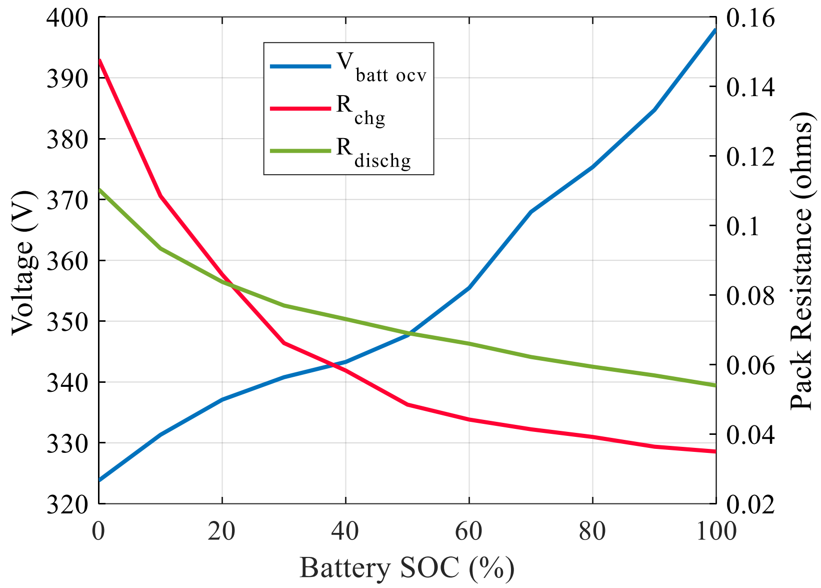

Figure 3- 4: Estimated/extracted battery pack parameters for the Chevrolet Bolt based on logged drive cycles

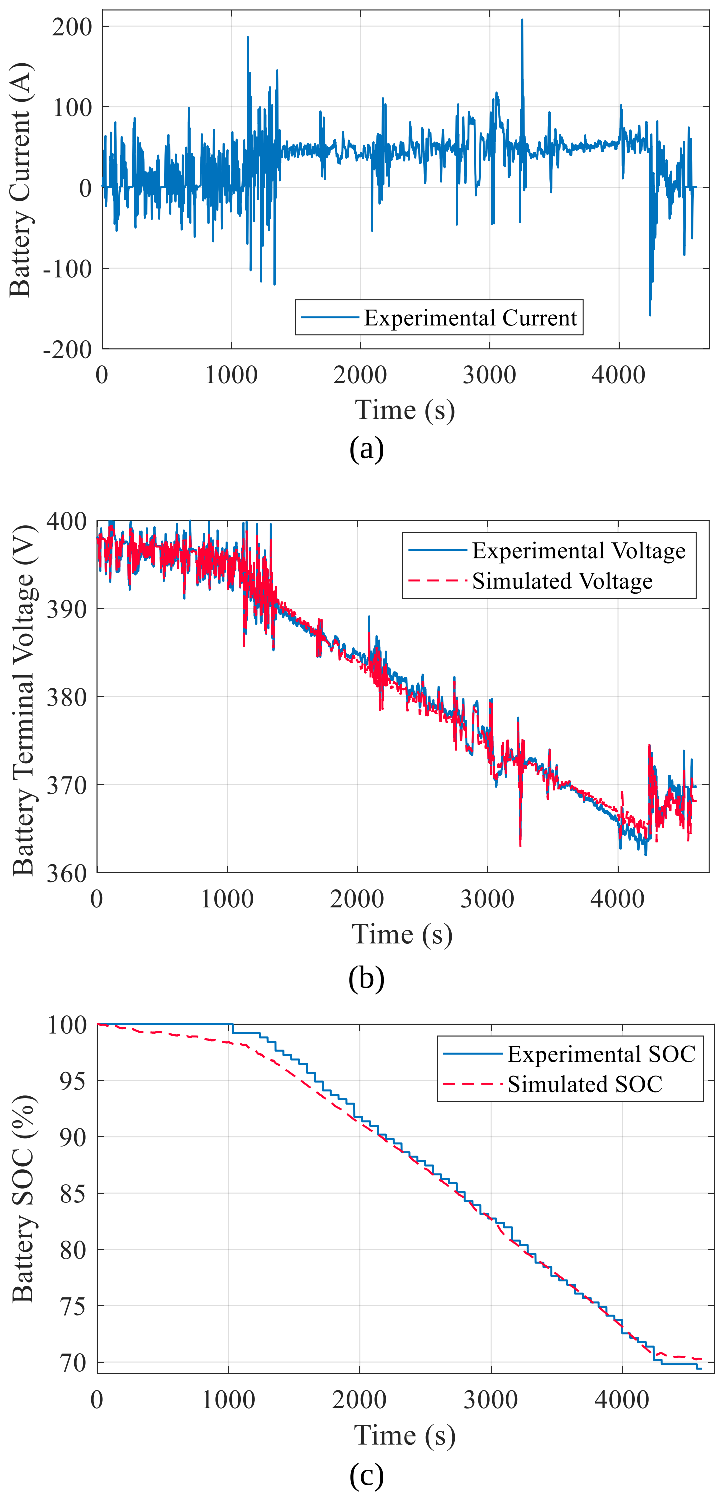

Figure 3- 5: Chevrolet Bolt battery model validation: (a) measured experimental current which is fed into battery model, (b) resulting simulated battery voltage

compared with experimental voltage, (c) resulting simulated battery SOC compared with experimental SOC

After the battery model is validated, the battery subsystem is added to the rest of the vehicle model for validation of the entire model. Fig 3-6 shows the four validation drive cycles, with the simulated speed matching closely to the experimental speed. Fig 3-7 compares the simulated battery SOC to the experimentally-logged battery SOC for each cycle. Table 3-2 summarizes the vehicle energy use difference between the model and the real vehicle, showing that all modeled results are within +/- 2.3% of the real vehicle, indicating a highly accurate BEV model.

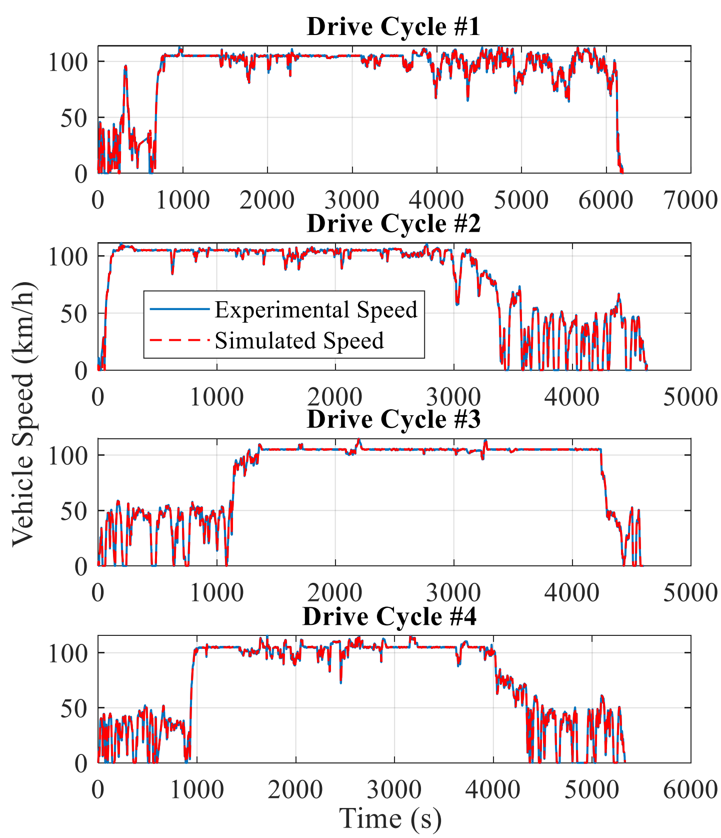

Figure 3- 6: Experimental and simulated drive profile for four validation drive cycles

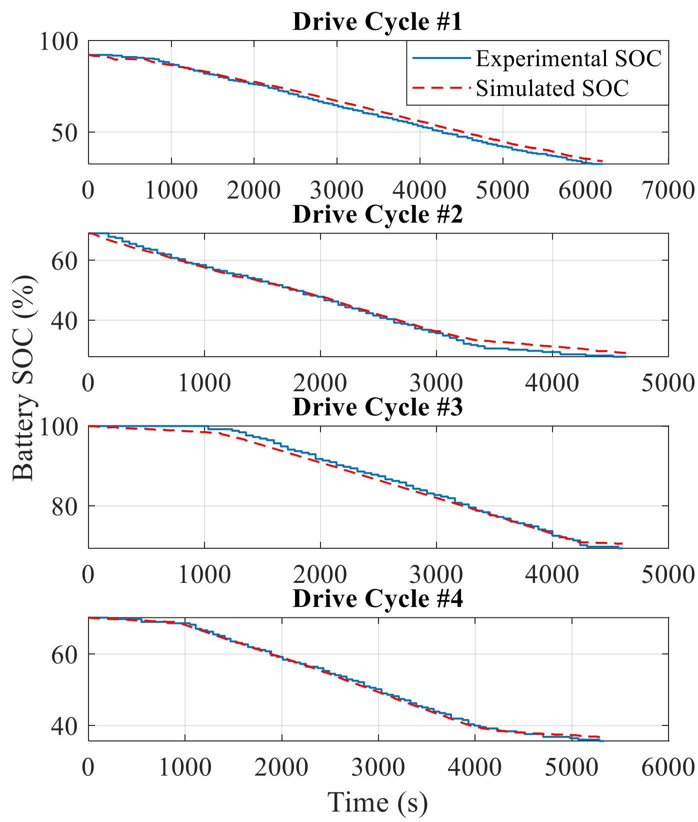

Figure 3- 7: Experimental battery SOC vs. simulated battery SOC for four validation drive cycles

TABLE 3-2: Vehicle Model Energy Usage Validation

Drive Cycle	Experimentally Measured Energy (kWh/km)	Simulated Energy (kWh/km)	Model Error (%)
# 1	0.1975	0.1997	1.11
# 2	0.2079	0.2031	-2.31
# 3	0.1641	0.1627	-0.87
# 4	0.1593	0.1603	0.66

3.3 FCREV Vehicle Model

The validated Chevrolet Bolt model is then modified to create the FCREV model, as shown in Fig 3-8. The fuel cell and associated DC/DC converter are connected to the high voltage bus, and the fuel cell can power the inverter/motor while driving and/or charge the battery.

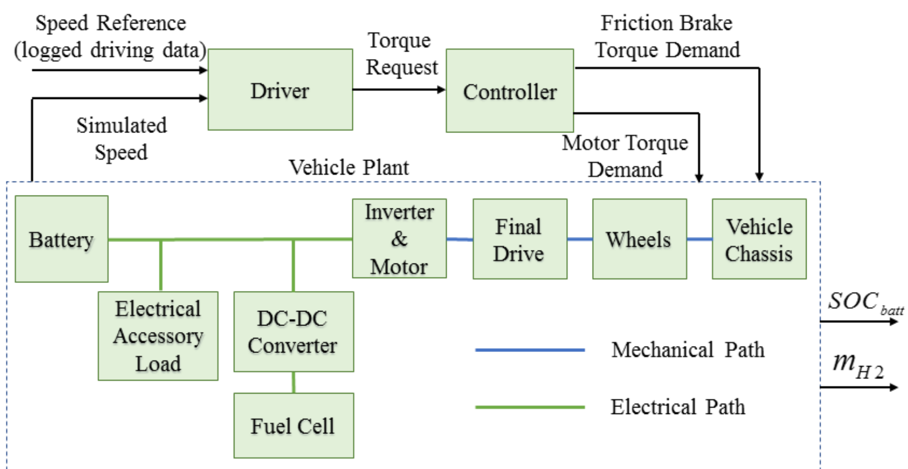

Figure 3- 8: Block diagram of FCREV model

In the battery block, the battery required current (I_{batt}) is the sum of the required motor current (I_{in_motor}) and the required electrical accessory current minus the current from the DC/DC converter connected to the fuel cell when it is turned on (I_{fc_dcdc}), as shown in (3-7). I_{in_motor} is positive for propelling and negative for regenerative braking. Equation (3-7) shows that during propelling, current from the fuel cell DC/DC converter will go directly to the motor, and the battery will provide any additional current required. If the current from the fuel cell-DC/DC converter system is greater than the required motor current, the fuel cell system current supplies all required current to the motor and the excess fuel cell system current charges the battery (negative I_{batt}). The electrical accessory current equals the electrical accessory power (P_{elec_access}) divided by the battery terminal voltage, V_{batt}. This vehicle electrical accessory load powers necessities like controllers, lights, windshield wipers, and heating/air conditioning. In this research, P_{elec_access} is set to 700 W to represent a small/moderate average accessory load, which has some low heating or air conditioning on for a portion of the trip. The voltage of the DC link connecting the battery and inverter is equal to V_{batt}, which will vary slightly over a drive cycle as the battery SOC changes and as the power into or out of the battery changes.

$$I_{batt} = I_{in\_motor} + \frac{P_{elec\_access}}{V_{batt}} - I_{fc\_dcdc} \tag{3 - 7}$$

Detailed experimental test results of the 2017 Toyota Mirai, obtained by Argonne National Laboratory [3], are used to model the efficiencies of the solid polymer electrolyte fuel cell and fuel cell DC/DC converter. The fuel cell is run at various steady power levels in 22 °C ambient temperature conditions to generate the efficiency curve and hydrogen is stored at 700 bar [3]. The DC/DC converter has a switching frequency of 9.55 kHz [3]. Since the rated power size of the fuel cell and converter changes in different optimization runs in this research, the efficiencies from [3] are presented as a function of operating power as a percent of rated power, as shown in Fig 3-9. The fuel cell DC/DC converter efficiency, η_{dcdc}, is shown by the red curve in Fig 3-9, and the fuel cell efficiency, which includes losses of the compressor and pumps, is shown by the blue curve. In each optimization run, the DC/DC converter rated power size is set to be equal to that of the fuel cell, and the efficiency is set based on the fuel cell operating power for that run. The fuel cell operating power, $P_{fc\text{-}op}$, is equal to the rated fuel cell power, P_{fc}, multiplied by the % of rated power operation, R_{fc}. Thus, I_{fc_dcdc} is calculated by (3-8).

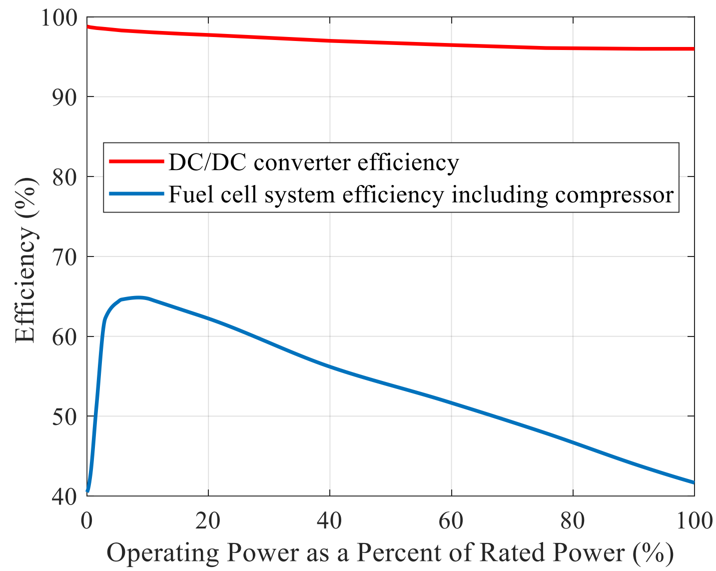

Figure 3- 9: Fuel cell system efficiency and fuel cell DC/DC converter efficiency over operating rated power [3]

$$I_{fc\_dcdc} = \frac{P_{fc-op}\eta_{dcdc}}{V_{batt}} = \frac{R_{fc}P_{fc}\eta_{dcdc}}{V_{batt}} \quad \textbf{(3 - 8)}$$

In this study, it is important to consider different fuel cell operating rates (R_{fc}) because using a higher rate such as 100% makes full use of the fuel cell cost, but exhibits lower efficiency at all times. If a lower operating power such as 60% or 80% is used, fuel cell efficiency is higher all day, but a larger fuel cell must be purchased to get the same net output power. Equation (3-9) uses η_{fc}, from Fig 3-9, to calculate the hydrogen used over the day, where t_{end} is the ending time of the day. The lower heating value (LHV_{H2}) of hydrogen is set at 1.2×10^8 J/kg [10].

$$m_{H_2}(t_{end}) = 1000 \times \int_0^{t_{end}} \left(\frac{P_{fc-op}(t)}{\eta_{fc} LHV_{H_2}} \right) \quad \textbf{(3 - 9)}$$

In this study, the battery energy capacity of the FCREV is varied between 30 kWh and 50 kWh, and the same 89.2% "useable" factor from the Bolt is applied. Thus, for every studied capacity, E_{batt}, the actual useable energy is $E_{batt,useable} = 0.892 \times E_{batt}$. When the battery is scaled to different capacities, it is assumed the V_{batt_ocv}-SOC curve remains constant, which physically means the number of cells in series remains the same. Thus, reducing the energy capacity represents reducing the number of battery cells in parallel. When this is done, the battery internal resistance is also scaled larger with a smaller E_{batt}, to correctly reflect the fact that a smaller battery with the same terminal voltage is composed of less battery cells in parallel, and thus exhibits a higher pack resistance compared to a larger battery. All changing component masses are accounted for, according to the values in Table 3-3, with linear scaling assumed.

TABLE 3-3: Component Mass in the 60 kWh Vehicle Model

Component	Mass (Unit)	Reference
Battery	440 (kg)	[37]
DC/DC Converter	6.4 (kW/kg)	[40]
Fuel Cell System	0.659 (kW/kg)	[41]
Hydrogen Tank	17.5 (kg/kg of H_2)	[42]

Chapter 4

Proposed Optimization Algorithm For WDDP-FCREVs

The optimization of hybrid vehicle design has been studied extensively, and numerous heuristic algorithms have been suggested [43], [44] which rely on a full vehicle simulation, but the simulation time is long and they can get trapped in local minims [45]. Some attempts have been made to overcome this obstacle, such as scripting only a portion of the vehicle model [46], which requires some approximations but accelerates the optimization process greatly. This thesis proposes an analytical algorithm that considers energy use and battery SOC for each driving trip or parked time within a day's driving schedule, rather than second-by-second calculations.

4.1 Proposed Offline Optimization Algorithm

The proposed algorithm is used offline during the vehicle design process to determine the component sizes (E_{batt}, P_{fc}, m_{H2}) and constant fuel cell power rate (R_{fc}) that provide the longest driving range for a given long-distance driving profile (i.e., one whole driving day including driving and parked times). Since the second-by-second vehicle simulations in Simulink take a considerable amount of time to run, the entire algorithm process is instead scripted as calculations which are much faster, so a simple exhaustive search of the three variables (E_{batt}, P_{fc}, R_{fc} – m_{H2} is dependent on E_{batt} and P_{fc}) can be used in the optimization process. The main input required is the average energy consumption (kWh/km) of each driving trip in the day for a corresponding BEV – this can be obtained from a single Simulink simulation or by using EPA ratings for standard cycles. The algorithm then steps through each driving trip and parked segment starting at the beginning of the day, with the assumption that it is a long-distance driving day, since this is the focus of the algorithm. Thus, the fuel cell is assumed to be on and generating power from the beginning of the first driving trip. On each driving trip, there is a change in battery energy from the traction/accessory energy used and the fuel cell energy generated – the algorithm calculates this change in energy for each driving trip. Similarly, there is a change in battery energy during each parked segment, but this is a net increase in energy if the fuel cell has been on and generating power for the whole parked segment, which will be the case unless the battery SOC reaches it maximum or the hydrogen tank becomes depleted. Thus, the algorithm steps through each driving trip and parked segment, adding or subtracting the battery energy change for each one to determine when the battery useable energy will be depleted. When the battery is depleted within a driving trip, linear approximation is used to find the point within that trip where the battery fully depletes, which indicates the range.

Fig 4-1 shows an example full-day test drive cycle with a total range of 704 km. This customized drive cycle is created by "sewing" together driving trips from a real-world driving dataset of 100 logged drivers from Toronto, Canada. Alternatively, test cycles can be created by sewing together standard cycles such as UDDS, HWFET, and US06. This customized test cycle is composed of 16 trips (driving segments) and 15 parked segments in between the trips. The driving trip segments and parked segments are defined by the key-on and key-off signals in the logged data, and thus a trip segment can include stopped times such as waiting at a red light. For the algorithm, the required drive cycle extracted information is: (1) each trip time in hours (t_{T1}, t_{T2}, t_{T3}, …), (2) each parked time in hours (t_{P1}, t_{P2}, t_{P3},…), (3) the average velocity of each trip segment (v_1, v_2, v_3,…), and (4) the average BEV energy consumption of each trip segment (c_1, c_2, c_3,…), where the BEV is chosen to have the same main vehicle parameters as the planned FCREV, such as the

Chevrolet Bolt in this study. The energy consumption of the i^{th} trip, c_i, can be obtained from the simulation of a full BEV model, or from EPA ratings for standard drive cycles (UDDS, HWFET, US06, etc.).

Though using the BEV energy consumption for each trip segment is reasonable, the accuracy of the results can be slightly improved by adjusting each c_i slightly based on the new vehicle mass for each combination of E_{batt}, P_{fc}, and m_{H2} for the FCREV. This can be accomplished using a two-dimensional look-up table with mass and average vehicle speed as inputs, where the table gives a % increase or decrease in c_i for each case, compared to the baseline BEV c_i. To generate this table in this study, shown in Fig 4-2, the BEV Simulink model was simulated on 40 real world logged trips (with a mix of city and highway trips) with varying vehicle masses. The Bolt BEV baseline mass is 1696 kg (including 80 kg driver weight). As expected, the % of energy use reduction with a smaller vehicle mass is lower at high speeds (highway driving) than at low speeds (city driving) because there is less $F=ma$ force required at cruising highways speeds, which is largely dependent on mass, compared to stop-and-go city driving. It is useful to note that many combinations of battery/fuel cell/tank sizes in the FCREV have lower mass than the baseline 440 kg 60 kWh battery in the BEV. Thus, one potential advantage of a FCREV is lower mass leading to lower energy consumption, which is accounted for in the algorithm using Fig 4-2, and is reflected in the optimization results.

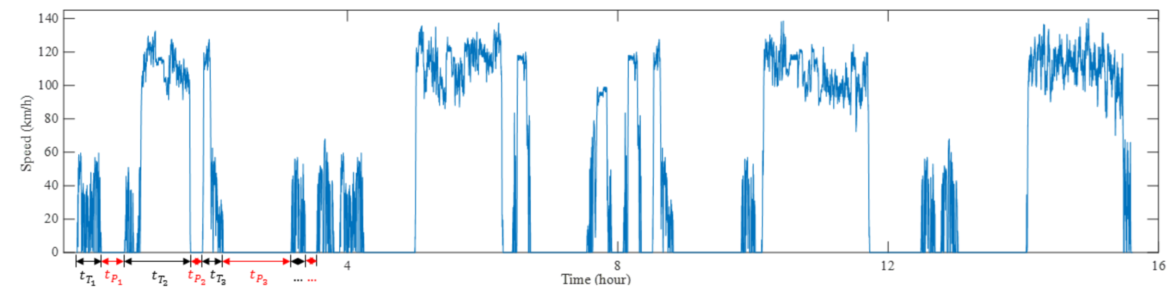

Figure 4- 1: A real-world logged test drive cycle for use in the analytical algorithm

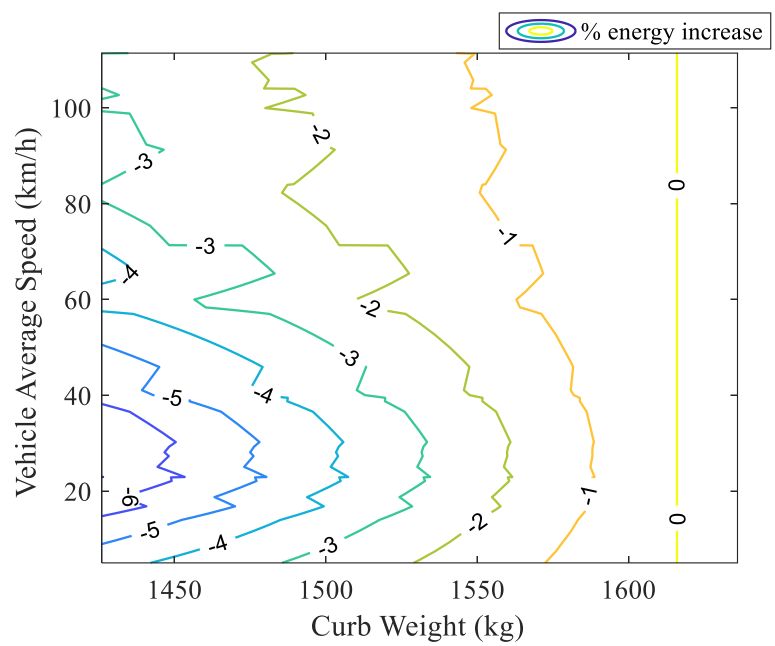

Figure 4- 2: Percentage of energy consumption increase with change in vehicle mass

In addition to the drive cycle extracted parameters, the algorithm also requires the cost of each component, which is scaled linearly as component sizes change. The costs used in this study are summarized in Table 4-1. The total cost, C_{total}, is set as a fixed input to the algorithm, so the longest range FCREV design can be found for a given cost by calculating the range for all variables of interest. For example, if C_{total} for the FCREV hybrid components is desired to be equal to the 60 kWh battery cost of the BEV Bolt, C_{total} =

\$9360. In this study, E_{batt} is stepped at intervals of 0.1 kWh between 30 kWh and 50 kWh and P_{fc} is stepped at intervals of 0.1 kW between 6 kW and 22 kW. The battery lower bound of 30 kWh is selected because is allows the vehicle to complete the whole day's driving needs with battery electric power on 97% of the logged driving days (1802 out of 1858 days). The hydrogen tank capacity is set based on the remaining cost from the optimization problem defined in (4-1). The algorithm is run for % of operating fuel cell power, R_{fc}, of between 50% and 100%, stepping in intervals of 5%. The goal is to find the maximum range, R, within the given constraints in (4-1).

$$\max R(E_{batt}, P_{fc}, m_{H2}, R_{fc}) \tag{4 - 1}$$

$$\text{s.t. } C_{total} = E_{batt}C_{batt} + P_{fc}(C_{fc} + C_{dcdc}) + m_{H2}C_{\tan k}$$

$$30kWh \le E_{batt} \le 50kWh$$

$$6kW \le P_{fc} \le 22kW$$

$$0.5 \le R_{fc} \le 1$$

TABLE 4-1: Component Costs

Component	Name	Cost (Units)	Reference
Battery	C_{batt}	156 (\$/kWh)	[47]
Fuel cell system	C_{fc}	45 (\$/kW)	[48]
DC/DC converter	C_{dcdc}	45 (\$/kW)	[49]
Hydrogen tank	C_{tank}	472.86 (\$/H_2 kg)	[50]

To calculate the daily range, R, the algorithm considers two cases: (1) the hydrogen tank is full at the start of the day and no refueling is possible during the day, and (2) the hydrogen tank is full at the start of the day and hydrogen refueling occurs every t_{refuel} hours, where t_{refuel} is a user input to the algorithm. In both cases, the battery is assumed fully charged at the start of the day from overnight charging the night before. The algorithm calculations are first described for the no refueling case below, and then are expanded for the refueling case.

First, the time that the fuel cell can run from the start of the first trip, t_{fc_total}, is calculated based on the hydrogen flow rate (Q_{H2} in kg/h) as shown in (4-2) and (4-3).

$$t_{fc\_total} = \frac{m_{H_2}}{Q_{H_2}} \tag{4 - 2}$$

$$Q_{H_2} = \frac{P_{fc-op} \times 3600000}{\eta_{fc} LHV_{H_2}} \tag{4 - 3}$$

Then a loop is run to calculate the change in energy, ΔE, of the battery after each trip segment and each parked segment. The change in battery energy for driving trip i, ΔE_{Ti}, is given by (4-4) where $t_{Ti\_fc\_on}$ is the time the fuel cell is on during this trip based on the amount of hydrogen left in the tank, and if the battery is fully charged. For example, $t_{Ti\_fc\_on}$ will equal t_{Ti} if there is enough hydrogen remaining to power the fuel cell for the entire trip i and the battery does not become fully charged; otherwise, $t_{Ti\_fc\_on}$ will be less than t_{Ti} according to one or both of these constraints. Similarly, the change in battery energy during parked segment i, ΔE_{Pi}, is given by (4-5), where $t_{Pi\_fc\_on}$ is the time the fuel cell is on during this parked segment based on the remaining hydrogen and battery SOC. Thus, $t_{Pi\_fc\_on}$ can be equal to or less than the time duration of parked segment i, t_{Pi}.

$$\Delta E_{Ti} = -c_i v_i t_{Ti} + (P_{fc-op}\eta_{dcdc})t_{Ti\_fc\_on} \tag{4 - 4}$$

$$\Delta E_{Pi} = P_{fc-op}\eta_{dcdc} t_{Pi\_fc\_on} \tag{4 - 5}$$

The ΔE_{Ti} and ΔE_{Pi} values are used to find the cumulative change in battery energy from the start of the day to the end of the k^{th} driving trip, $\Delta E_{end,Tk}$, as shown in (4-6). Equation (4-6) considers k-1 parked segments because only k-1 parked segments have occurred prior to the k^{th} trip.

$$\Delta E_{end,Tk} = \sum_{i=1}^{k} \Delta E_{Ti} + \sum_{i=1}^{k-1} \Delta E_{Pi} \tag{4 - 6}$$

The algorithm then checks which is the first trip to have cumulative battery energy use, $\Delta E_{end,Tk}$, greater than the useable battery energy, $E_{batt,useable}$. The battery will deplete at some point in this trip, and thus driving range is determined in this trip. The algorithm estimates the range within this trip, say trip k, using the ratio of remaining battery energy for use in this trip to the total energy needed for the trip, as shown in (4-7). Thus, the algorithm assumes a constant energy consumption rate, c_k, over the trip, which is a required approximation to speed up the calculation time so significantly. In (4-7), d_i is the distance of trip i, which is calculated using the drive cycle extracted parameters of trip average velocity and trip time, shown in (4-8).

$$R = \sum_{i=1}^{k-1} d_i + d_k \left(\frac{E_{batt,useable} + \Delta E_{end,Tk-1} + \Delta E_{Pk-1}}{-\Delta E_{Tk}} \right) \tag{4 - 7}$$

$$d_i = v_i t_{Ti} \tag{4 - 8}$$

In the refueling case, the algorithm checks if the hydrogen tank can be refueled at the beginning of each trip segment and parked segment. Once the accumulated total driving and parking time passes t_{refuel}, the tank is set to full again, and the range calculation considers the extra hydrogen added. If the whole day's trip (maximum range) can be achieved for various size combinations, the algorithm can decrease the initial vehicle cost, C_{total}, and run the loop again to find those component combinations which still meet the maximum range requirement, but at a lower vehicle cost. Thus, the scripted algorithm can find the optimal component size and fuel cell control that meets the driving range needs and has the lowest cost. The algorithm is implemented as a MATLAB script. Fig 4-3 summarizes the algorithm steps at a high level to find the maximum range for a given total cost, C_{total}. Fig 4-4 shows the detailed steps to calculate range for both the refueling case and the non-refueling case. Overall, the algorithm uniquely allows for a fast estimation of total range on any test drive cycle, meaning all combinations of battery size, fuel cell size, and fuel cell operating power can be quickly considered in an exhaustive search. The fast calculation speed of the algorithm allows more design loops of interest to be run, such as changing C_{total} or changing the vehicle accessory power, as will be illustrated in Chapter 5.

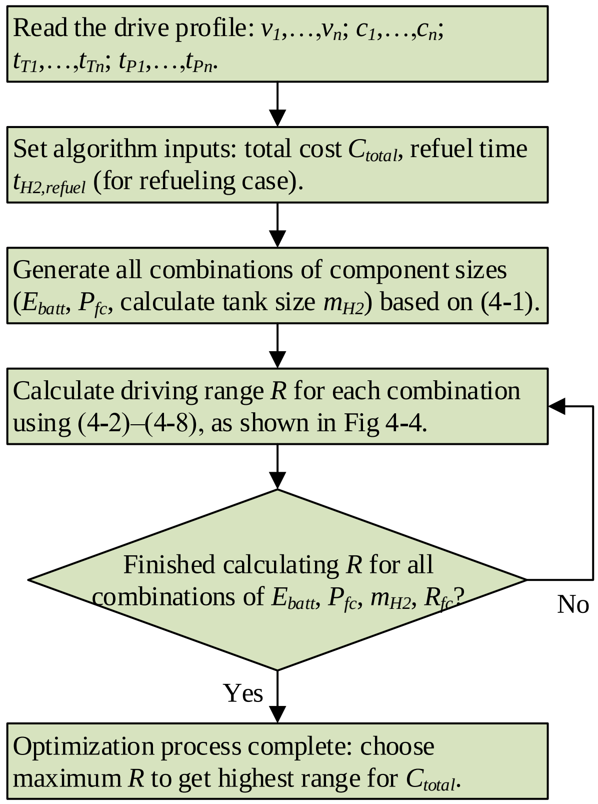

Figure 4- 3: High-level summary of proposed offline optimization for FCREV design

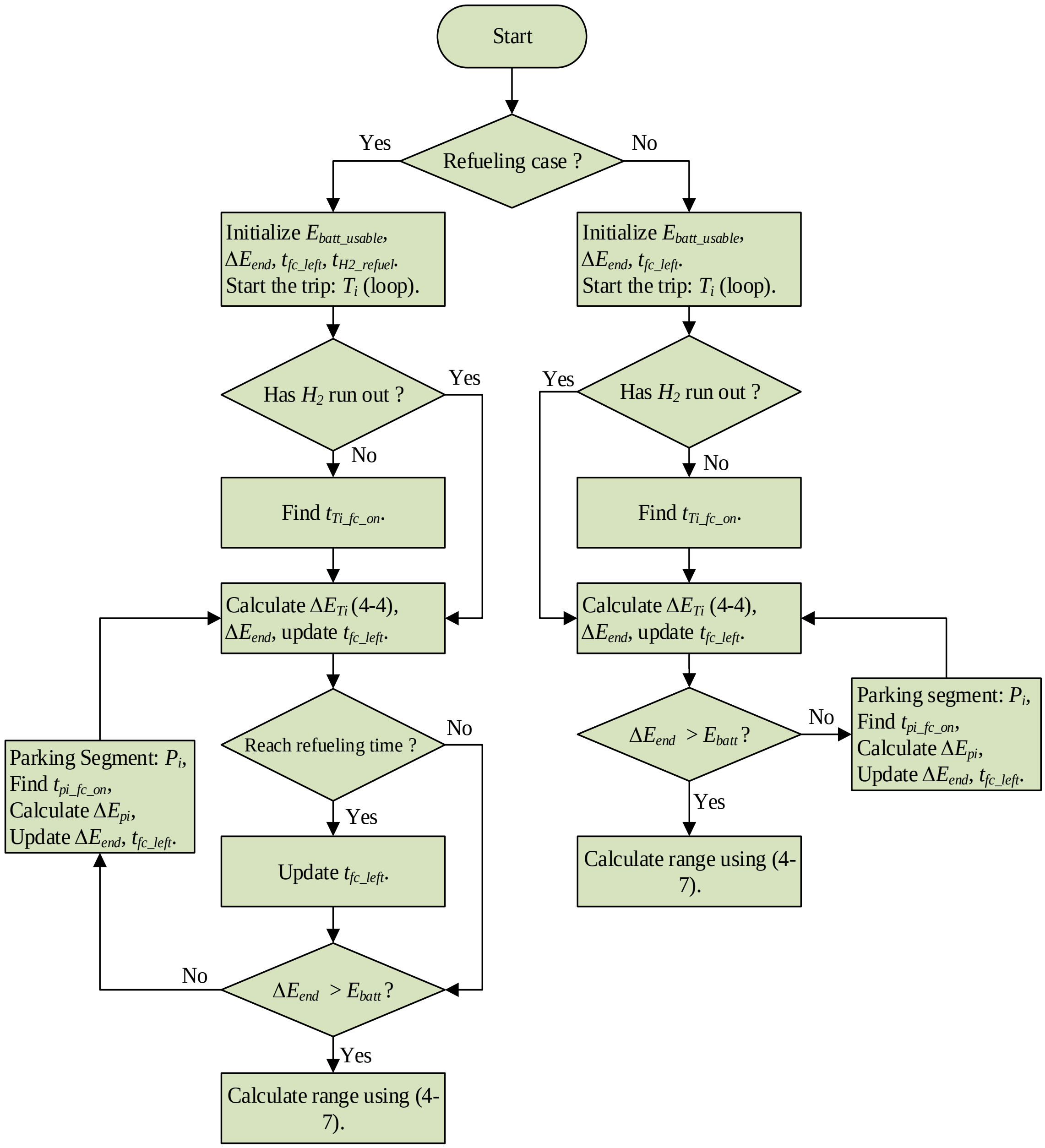

Figure 4- 4: Detailed steps for calculating range in the algorithm for each combination of component and control options

4.2 Algorithm Validation

To validate the accuracy of the proposed algorithm, the full Simulink model of the WDDP FCREV is run on the drive cycle in Fig 4-1 with larger component step sizes for both no refueling and refueling cases. Fig 4-5 shows the battery SOC for the simulated Bolt BEV with 60 kWh battery, the simulated FCREV with WDDP strategy, and the algorithm-scripted FCREV with WDDP strategy, where both FCREV cases use a 30 kWh battery, a 9 kW fuel cell running at 100% power, and no hydrogen refueling. Fig 4-5 shows the large range extension that is possible using a small 9 kW fuel cell with the WDDP control strategy compared to a BEV of the same cost. Fig 4-5 also shows that the simulated FCREV SOC aligns closely with the much faster algorithm-based FCREV SOC calculations, which occur at the end of each driving or parked segment.

Fig 4-6 shows the percentage error of driving range between the simulated FCREV model and the algorithm FCREV for the no refueling case, where the battery step size is 5 kWh, the fuel cell step size is 1 kW, and R_{fc} = 100%. The results for the refueling case are very similar to those shown in Fig 4-6. The % range error between the scripted algorithm and full simulation is generally very small, usually less than 1%, and less than 3.6% for all component size combinations. The general accuracy of the algorithm over the whole search space is very high and gives reliable results.

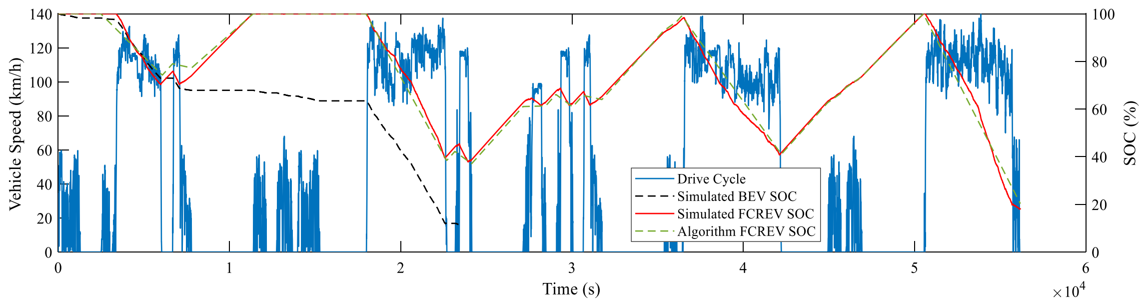

Figure 4- 5: Battery SOC comparison between simulated vehicle models and scripted algorithm

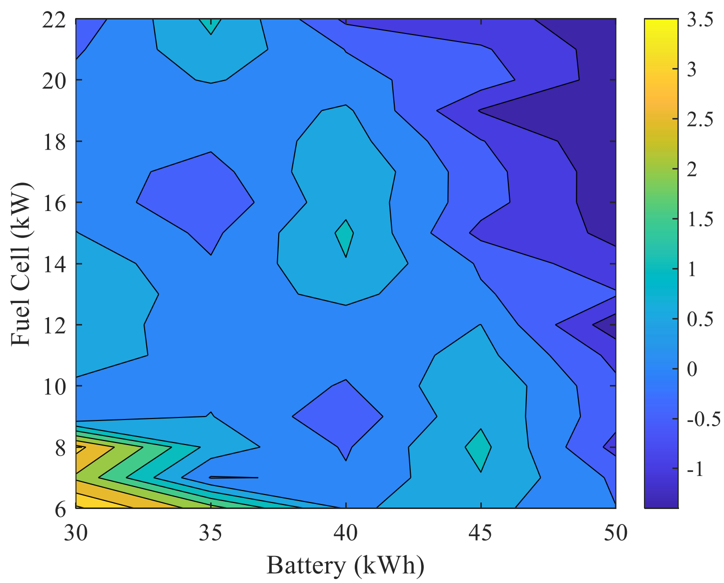

Figure 4- 6: Absolute value of percentage difference between driving range resulting from full vehicle model and algorithm (no refueling, 100% fuel cell power)

Chapter 5

Design Optimization Results

5.1 Customized Drive Cycle Optimization Results

For the customized drive cycle shown in Fig 4-1, the Bolt BEV model achieves 280 km of range with a 60 kWh battery for an energy storage cost of $9360. For the same cycle and cost, the optimization algorithm is run for battery size 30 kWh to 50 kWh (in steps of 0.1 kWh), fuel cell size 6 kW to 22 kW (in steps of 0.1 kWh) and fuel cell operating power, R_{fc}, from 50% to 100%, in 5% steps. All investigated values of R_{fc} had at least one component size combination that could complete the full cycle range of 704 km. Thus, an optimal WDDP-FCREV can drive 424 km further than the compared BEV on this cycle (with the same energy storage cost), which is a 151% increase in range. Since the full cycle can be achieved by any value of R_{fc}, the most preferrable R_{fc} is that which gives the largest number of component combinations that meet the full range, indicating it can easily achieve the driving range for a variety of component sizes. In this case, the optimal R_{fc} = 75% for the no refueling scenario, and these algorithm results (driving range in km) for the WDDP-FCREV are shown in Fig 5-1(a). For this case, the full driving range is achieved for fuel cell sizes from 11 kW to 16 kW and battery sizes 30 kW to 33 kW. For example, one optimal point in this plot is a 12 kW fuel cell, a 31 kWh battery, and a 7.3 kg hydrogen tank. For comparison, Fig 5-1(b) shows the results for R_{fc} = 100%, where the optimal component sizes are a 9 kW fuel cell, a 30 kWh battery, and a 8.2 kg hydrogen tank. The higher fuel cell efficiency at 75% of rated power means there is a more efficient use of on-board hydrogen energy, so a smaller tank can be used, but a larger fuel cell is required.

For the refueling case, where t_{refuel} is set to 4 hours, Fig 5-2(a) shows the optimal R_{fc} value is 100% as it gives the largest number of component combinations that can meet the full range, though lower values can also meet the full range. For example, a 9 kW fuel cell, 30 kWh battery, and 8.2 kg tank can meet the full range, as can a 14 kW fuel cell, 45 kWh battery, and 2.3 kg tank. This shows a much smaller tank can be used since the vehicle can refuel part-way through the day. Fig 5-2(b) shows another example with R_{fc} = 60%, where the range can still easily be met by a variety of component sizes, but a larger fuel cell is generally needed.

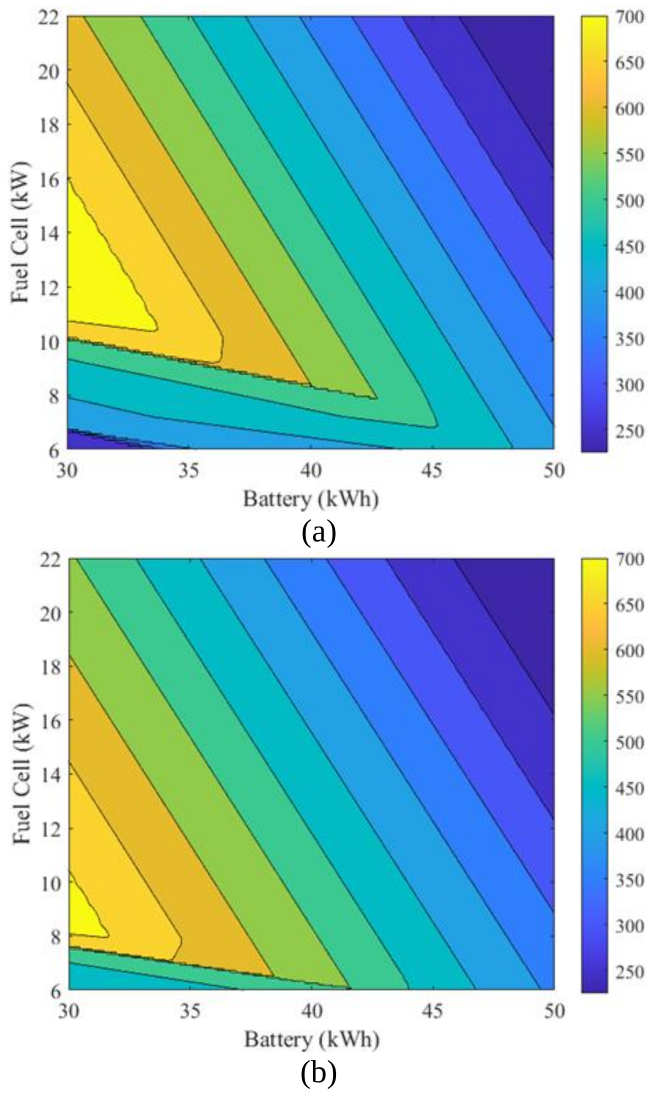

Figure 5- 1: Algorithm range results (in km) for no refueling: (a) 75% fuel cell power (optimal); (b) 100% fuel cell power (for comparison)

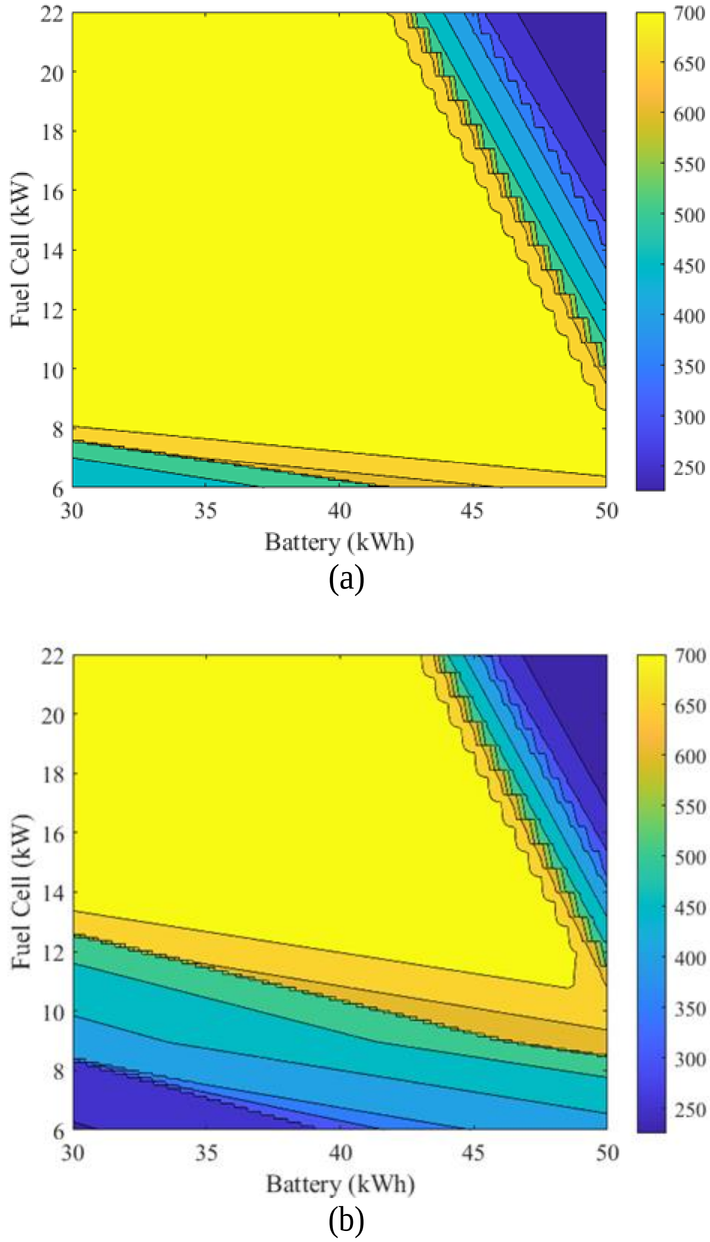

Figure 5- 2: Algorithm range results (in km) for refueling: (a) 100% fuel cell power (optimal); (b) 60% fuel cell power (for comparison)

5.2 Real-World Drive Cycle Optimization Results

The customized drive cycle was used with the scripted algorithm to show how a designer can create various test drive cycles by sewing together the desired drive cycles and parking segments. In this subsection, the algorithm is tested using the three longest real-world driving cycles from a logged dataset of 100 drivers in Toronto, Canada, where each driver was logged for 2 to 6 weeks using a CANbus datalogger. These cycles are "worst case scenarios" for a WDDP-FCREV since there is very little parked time, especially early in the cycle, which is crucial for fuel cell recharging of the battery. Fig 5-3 shows these three longest cycles, with daily ranges of 966 km, 943 km, and 801 km, all of which have a significant amount of highway driving.

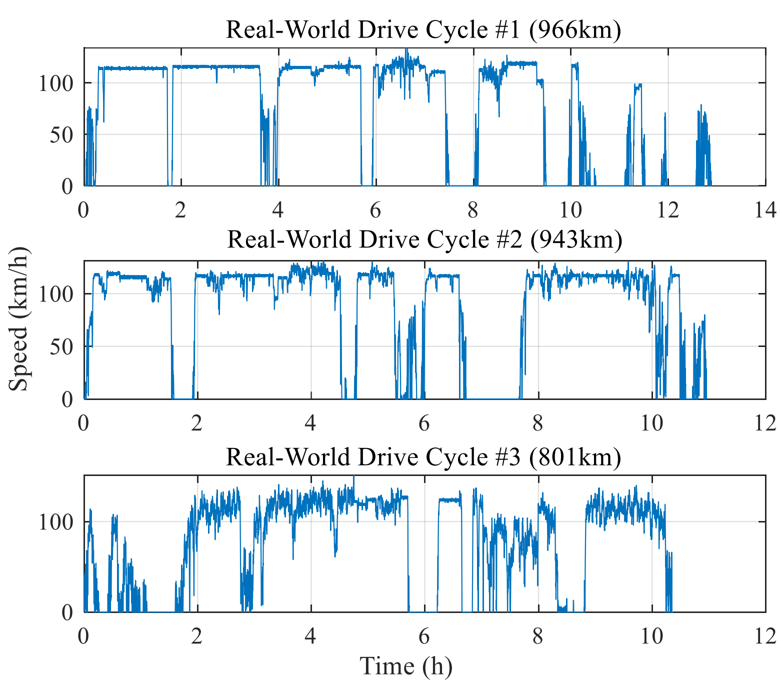

Figure 5- 3: Real-World drive cycles

Table 5-1 shows the maximum range achieved on the three real-world cycles for R_{fc} from 85% to 100%, as the lower R_{fc} values did not perform as well on these more aggressive cycles. For Cycles 1 and 2, the optimal R_{fc} is 90%, and for Cycle 3 it is 100%, leading to the general conclusion that on more aggressive high-speed cycles, a high R_{fc} around 90% to 100% is optimal, for the given fuel cell efficiency curve. The optimal FCREV without refueling is unable to complete the full range for the 3 cycles, whereas the optimal FCREV with 4-hour refueling can complete the full range on Cycles 2 and 3, and is unable to complete Cycle 1. However, when comparing to the BEV simulated range on these cycles (shown in the first column), Table 5-1 shows that for the same cost, the WDDP-FCREV can increase range by 100% to 120% with no hydrogen refueling in the day and by 144% to 245% if hydrogen refueling is assumed every 4 hours. These range increases are significant and could be an important factor in encouraging driver uptake of zero-emission vehicles.

Figs 5-4 and figure 5-5 show the optimal component sizing results for Cycle 1 with R_{fc} = 90% for the no refueling and refueling cases, respectively. For both cases, an optimal sizing combination is an 18.4 kW fuel cell, 30 kWh battery, and 6.4 kg hydrogen tank. It is useful to have a larger fuel cell on these higher speed cycles since the average power demands are higher. Figs 5-6 and figure 5-7 show the optimal component sizing results for Cycle 2 with R_{fc} = 90% for the no refueling and refueling cases, respectively. On Cycle 2, the ability to refuel makes a large difference, increasing range from 591 km to 940 km. An optimal sizing combination for both cases is an 18 kW fuel cell, 30 kWh battery, and 6.5 kg hydrogen tank. Figs 5-8 and figure 5-9 show the optimal component sizing results for

Cycle 3 with R_{fc} = 100%. The optimal sizes are around 18 kW fuel cell and 30 kWh battery for the no refueling case, but the refueling case has a much larger variety of sizes that allow the full 801 km range to be achieved, including a 15 kW fuel cell, 36 kWh battery, and a 5.1 kg hydrogen tank. It is useful to note that these results are somewhat different than those for the customized drive cycle (with lower speeds and more parked time), where an 18 kW fuel cell was far from optimal for the no refueling case, and a smaller fuel cell around 11 to 15 kW was preferred, to allow for a larger hydrogen tank within the fixed cost. This highlights the importance of using the fast algorithm on a wide variety of cycles, to fine-tune the optimal design for the expected cycles.

TABLE 5-1: Maximum Simulated WDDP-FCREV Range on Real-World Cycles

Drive Cycle	R_{fc}	Max Range (km) (no refueling)	Max Increase over BEV (no refueling)	Max Range (km) (refueling)	Max Increase over BEV (refueling)
Cycle #1=966km BEV range=272km	100%	593.10	119%	658.91	144%
	95%	594.72		663.93	
	90%	594.90		663.97	
	85%	594.16		661.49	
Cycle #2=943km BEV range=273km	100%	589.90	117%	943.00	245%
	95%	591.27		943.00	
	90%	591.61		943.00	
	85%	591.44		943.00	
Cycle #3=801km BEV range=272km	100%	556.50	105%	801.00	194%
	95%	556.45		801.00	
	90%	555.27		801.00	
	85%	553.45		801.00	

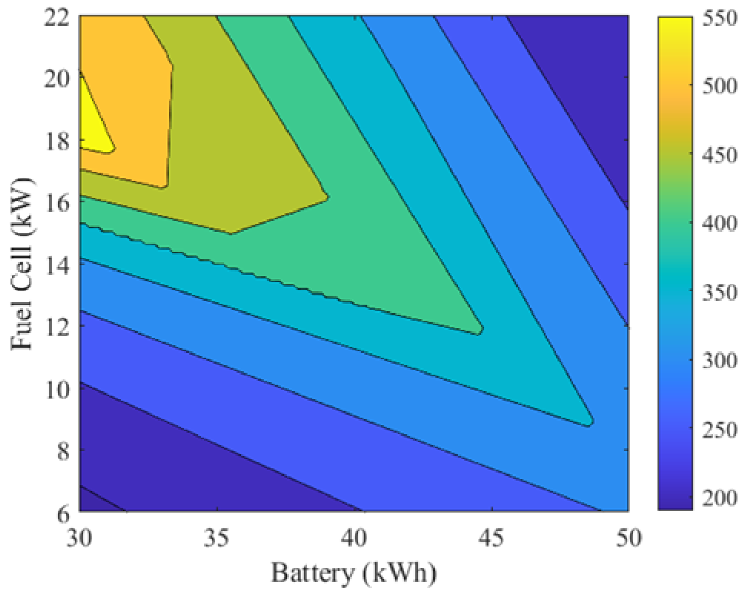

Figure 5- 4: Algorithm range results (in km) for Cycle 1 (no refueling, R_{fc} = 90%)

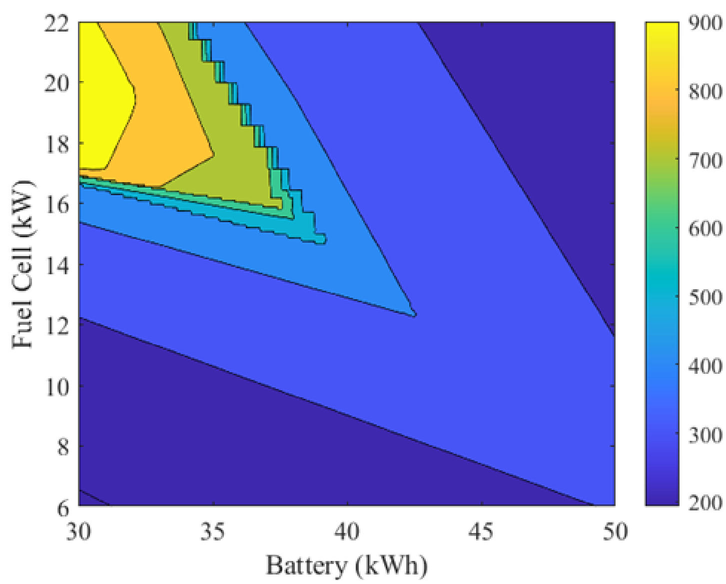

Figure 5- 5: Algorithm range results (in km) for Cycle 1 (refueling, Rfc = 90%)

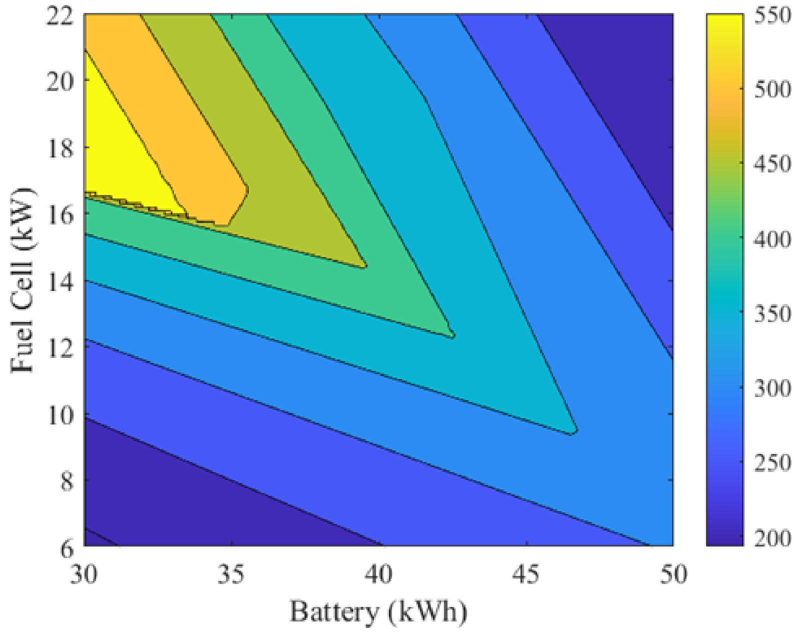

Figure 5- 6: Algorithm range results (in km) for Cycle 2 (no refueling, R_{fc} = 90%)

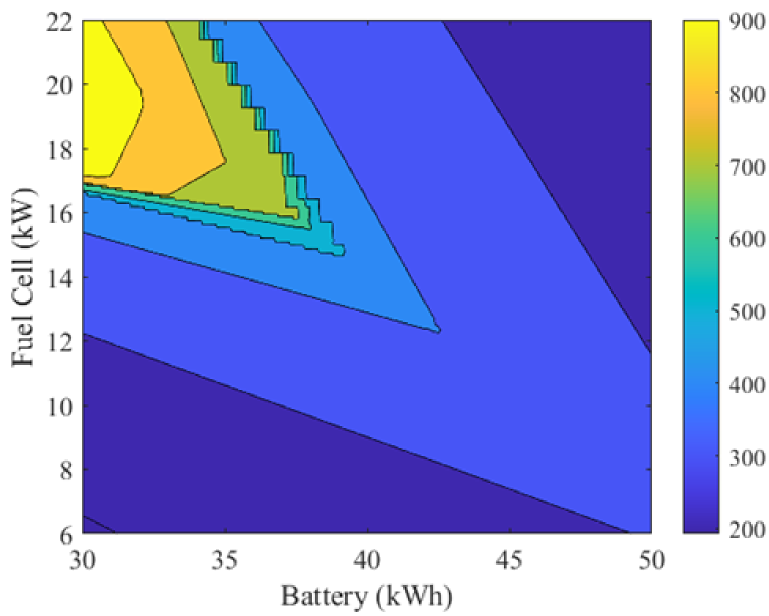

Figure 5- 7: Algorithm range results (in km) for Cycle 2 (refueling, R_{fc} = 90%)

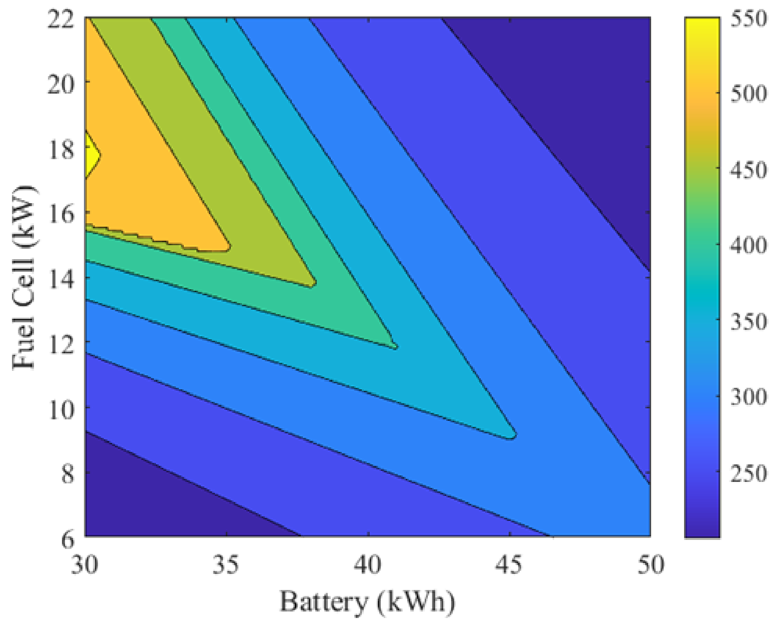

Figure 5- 8: Algorithm range results (in km) for Cycle 3 (no refueling, R_{fc} = 100%)

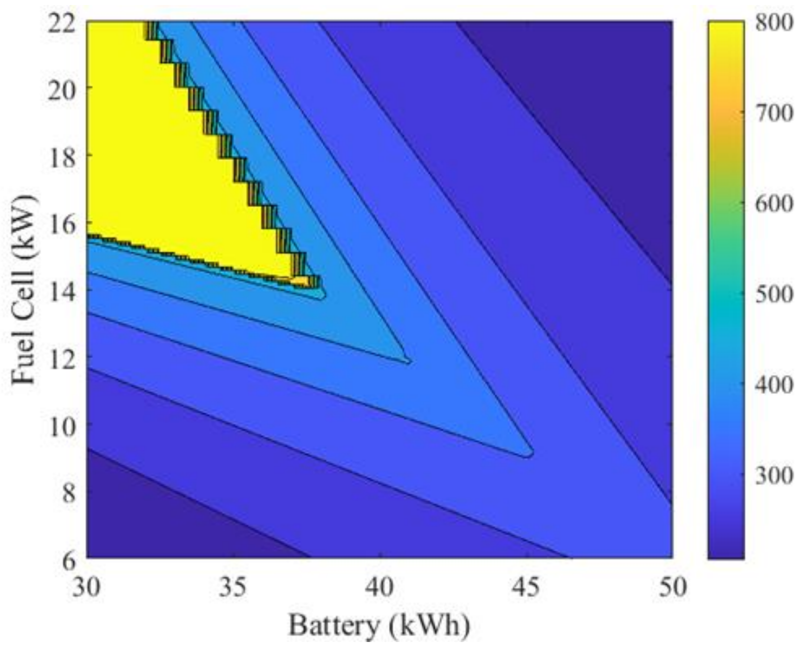

Figure 5- 9: Algorithm range results (in km) for Cycle 3 (refueling, R_{fc} = 100%)

Fig 5-10 shows the simulated battery SOCs for three cases on Cycle 2: full vehicle BEV model, full vehicle WDDP-FCREV model, and algorithm WDDP-FCREV, where the FCREV is refueled every 4 hours and has a 30 kWh battery, 18 kW fuel cell, and R_{fc} = 100%. These results further validate that the optimal size/control parameters found using the algorithm give similar range results as the full vehicle model. The green circles represent the "calculation points" in the algorithm (at the end of each driving or parked segment) to highlight the fact that even though the algorithm SOC (green) does not always track the full simulated SOC (red) due to averaging over each segment, the calculation points are quite accurate and lead to the correct daily driving range.

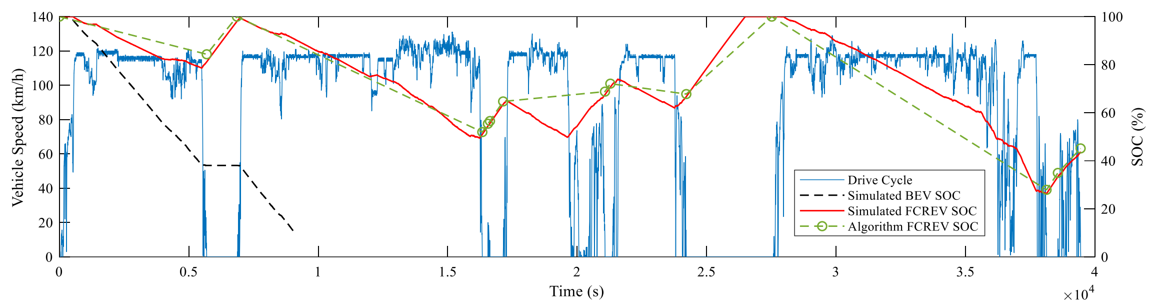

Figure 5- 10: Battery SOC comparison between simulated vehicle models and algorithm on real-world Cycle 2 (WDDP-FCREV has 30 kWh battery, 18 kW fuel cell, R_{fc} = 100%)

5.3 Optimization Sensitivity to Cost

The fast speed of the proposed optimization algorithm makes it useful to examine optimal results for a variety of cost scenarios. This subsection presents results for two cost sensitivity studies: i) some component costs are increased by 50%, and ii) total energy storage cost is reduced below that of the BEV.

Since the optimization algorithm is constrained by component costs, and costs can vary in different scenarios (such as different purchase quantities or reductions in the future), an additional optimization is run for the customized drive cycle where the fuel cell and dc/dc converter costs are increased by 50% compared to those in Table IV. Fig 5-11 shows the no refueling range results for the optimum R_{fc}, 85%. The optimal WDDP-FCREV with 50% higher fuel cell and dc/dc converter costs achieves a maximum range of 697 km with a 30 kWh battery, 10 kW fuel cell, and a 7.0 kg H_2 tank. This design nearly completes the full 704 km cycle, and drives 417 km (149%) farther than the baseline BEV. Compared to the results in Fig 5-1(a) with the original costs, the optimal fuel cell size has moved from a wide range of 11 kW to 15 kW down to 10 kW.

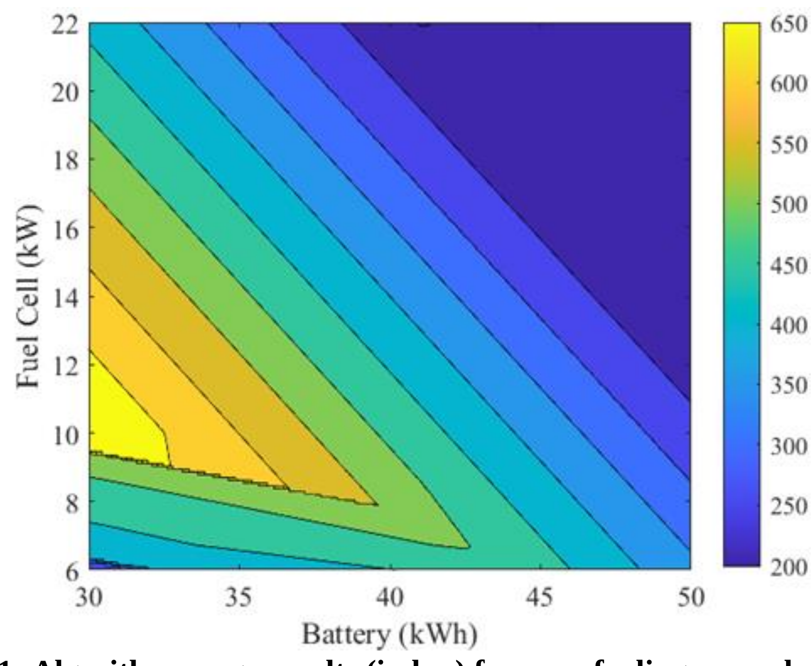

Figure 5- 11: Algorithm range results (in km) for no refueling case where fuel cell and dc/dc costs are increased by 50% (Optimal R_{fc} = 85%)

If the entire WDDP-FCREV energy storage cost is reduced to a fraction of the original BEV energy storage cost of $9360, the algorithm can be used to investigate the range achievable with an optimal WDDP-FCREV vehicle that is lower cost than the baseline BEV. Fig 5-12 shows this result for the three real-world logged cycles with standard component costs, where the algorithm loops are run at 70% to 100% of the BEV cost in steps of 1%. Each point on the plot is for the optimal battery size, fuel cell size, and fuel cell operating power for that cost, so this plot represents many different component and control results. Each cycle is represented by a unique color and since the BEV ranges on these cycles are within 1 km of each other, the average BEV range (272 km) is represented by the black horizontal line for comparison (at the usual 100% BEV cost).

For Cycle 1 (blue lines), since the cycle has near-constant high-speed driving at the start of the day, the battery depletes so quickly that the vehicle doesn't have a chance to refuel hydrogen before the battery is depleted; thus, the refuel and no refuel maximum ranges are the same. The optimal WDDP-FCREV range equals that of the BEV when the WDDP-FCREV energy storage cost is 73% that of the BEV, or $6833. Thus, this type of analysis can help the designer balance the competing goals of reducing cost and increasing range. For example, on Cycle 1, for 90% of the BEV cost, the WDDP-FCEV achieves a 455 km range, which is a 69% increase over the BEV at 100% cost. For Cycle 2 (red lines), the optimal WDDP-FCREV at 74% of the BEV cost equals the BEV range. For this case, Fig 5-12 shows that if the WDDP-FCREV cost is set to 90% or higher, significant gains in range can be achieved in the refueling case, with a 733 km range achievable at 90% cost and a 940 km range achievable at 100% cost. For Cycle 3 (green lines) the optimal WDDP-

FCREV range equals the BEV range when the WDDP-FCREV energy storage cost is 78% that of the BEV. Also, the WDDP-FCREV refueling case can complete the whole cycle (801 km) if the cost is 92% that of the BEV. Thus, the fast optimization script is useful to perform cost sensitivity analyses.

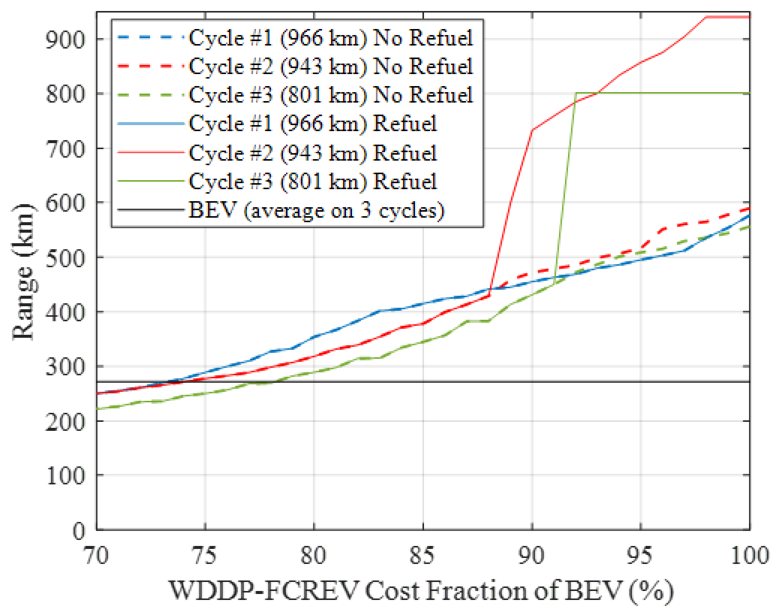

Figure 5- 12: Optimal WDDP-FCREV range results for energy storage costs 70% to 100% of the BEV cost

5.4 Optimization Sensitivity to Accessory Load

The preceding results used a 700 W accessory load, which is a low-to-moderate load. This section investigates the optimal WDDP-FCREV designs and ranges achieved on real-world Cycle 2 if the average accessory loads are increased to 1200 W and 2000 W, representing moderate loads which include some heating or air conditioning. The baseline BEV model is also run again with these higher accessory loads to obtain the BEV range achievable for each case. Fig 5-13 shows optimal component sizing results for the no refueling 2000 W load case, at the optimal fuel cell power of R_{fc} = 90%. For this case, the maximum range achieved by the WDDP-FCREV is 554 km with an 18 kW fuel cell, 30 kWh battery, and 6.5 kg tank, compared to the BEV range of 257 km. Fig 5-14 shows the trend of range decreases for each type of vehicle (BEV, optimal WDDP-FCREV without refueling, and optimal WDDP-FCREV with refueling) as vehicle accessory loads increase from 700 W to 2000 W. The results show that similar range increases can be expected at these higher loads as those at the lower original load of 700 W, with no refueling range gains around 115% and refueling range gains around 250%.

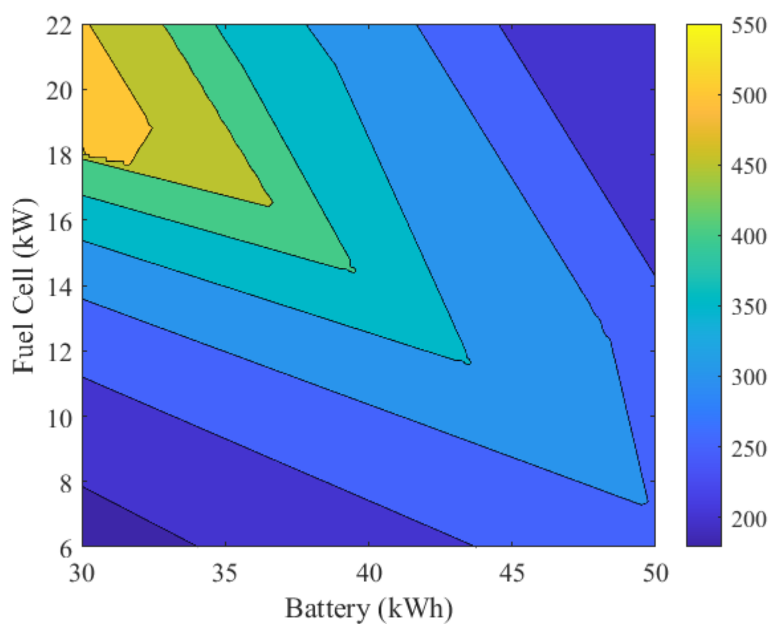

Figure 5- 13: Algorithm range results (in km) for no refueling case with accessory loads = 2000 W and optimal R_{fc} = 90%

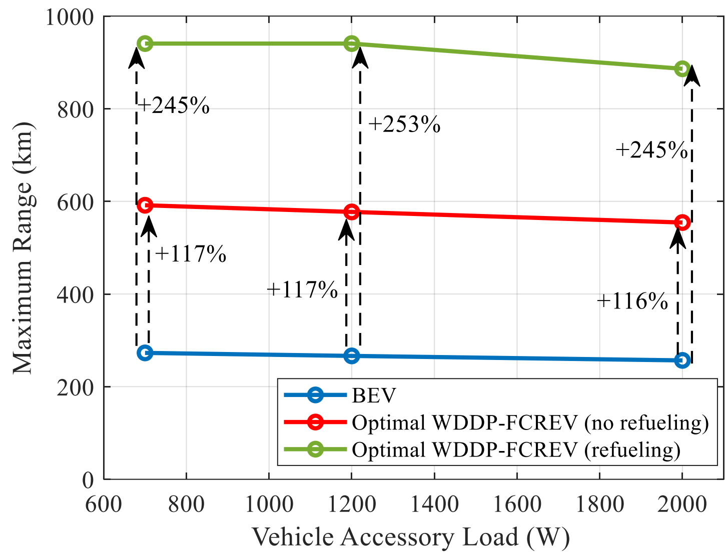

Figure 5- 14: Maximum achievable range on real-world Cycle 2 with 700W, 1200W, 2000W vehicle accessory loads

5.5 Comparison to BEV Fast-Charging

A main advantage of hydrogen refueling over BEV fast-charging is that hydrogen refueling can be completed in about 5 minutes [51], which is similar to what drivers are accustomed to for refueling gasoline-powered vehicles, and which does not materially interrupt the trip, assuming a H_2 filling station is available on the route. It is well-known that if a BEV is charged for long enough (say 20 to 60 minutes or more, depending on the charging power and battery size) and often enough, it could continue driving as long as needed. Hence, this subsection investigates the effect of BEV fast-charging on range for the 5 minute interval of H_2 refilling, to enable direct comparison with the WDDP-FCREV. The investigation considers the 3 real-world drive cycles, 50/100/150 kW fast-charging power levels, and refueling intervals (t_{refuel}) of 2 and 4 hours. The battery I^2R losses during fast-charging are accounted for according to the battery internal resistance shown in Fig 3-4.

The simulated results are shown in Fig 5-15. For the no refuel/recharge case, only a single BEV range value is given (green bar). The results show that short 5 minute recharges for BEVs, even at 150 kW every 2 hours, do not have a significant impact on range compared to the long ranges achieved by the WDDP-FCREV. For Cycles 1 and 2, the BEV recharges every 4 hours have no effect on the range because the battery has been fully depleted before the 4-hour mark, so the vehicle is unable to reach the recharge point. For all cycles, the WDDP-FCREV can complete the entire range when refueling every 2 hours is possible. The underlying benefit of the WDDP-FCREV is the large amount of energy stored in the vehicle at the start of the day, and this cannot be compensated for by short fast-charging events by the BEV. The results show that, for the common charging powers studied, BEVs need to rely on significantly longer charging times to attempt to complete the same distance in a day as the optimized WDDP-FCREV, which can interrupt trips and inconvenience drivers.

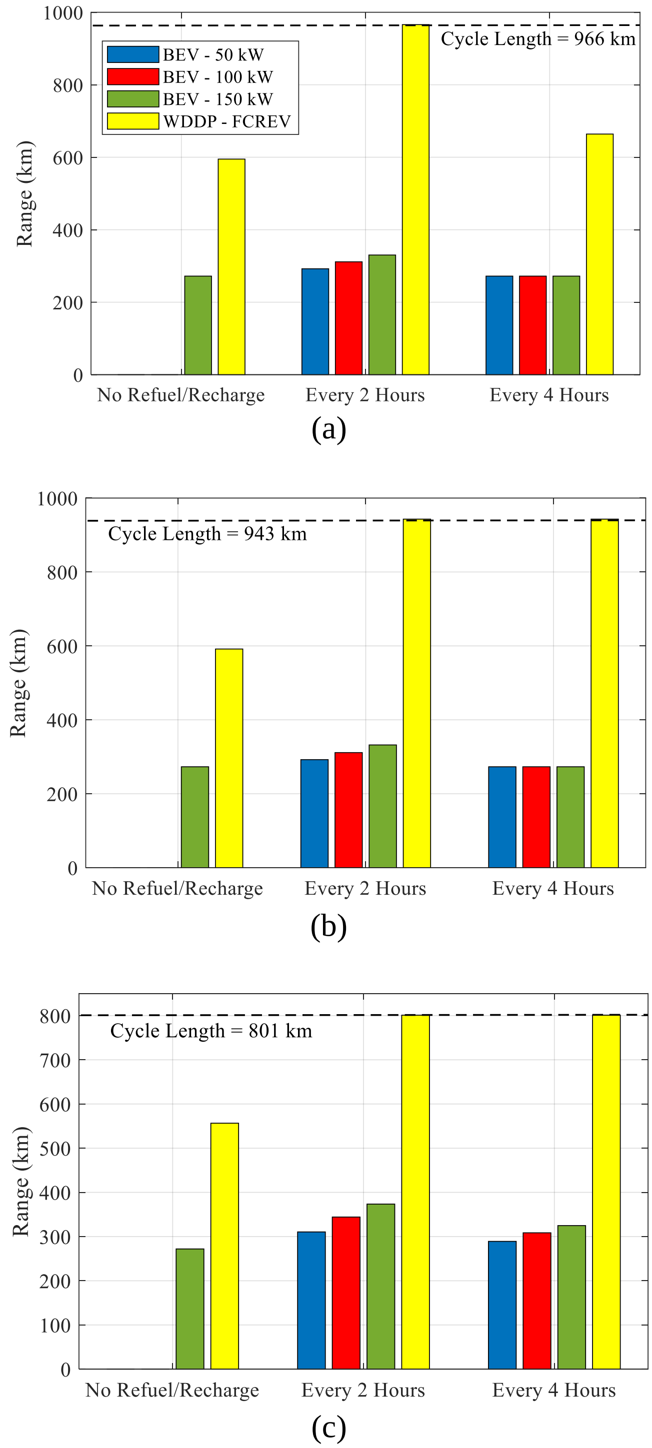

Figure 5- 15: BEV fast-charging results compared to WDDP-FCREV for (a) Cycle 1, (b) Cycle 2, and (c) Cycle 3

5.6 Optimization for Multiple Drive Cycles

The WDDP-FCREV analysis has thus far focused on one customized drive cycle and 3 real-world logged drive cycles. The proposed analytical design optimization algorithm gives fast and accurate results for the optimal fuel cell size, battery size, H_2 tank size, and fuel cell percentage power level for the target drive cycle. However, in the real design process, one optimal design must be selected in the design phase to work well with a wide variety of potential drive cycles. Thus, this subsection proposes a simple method to determine the optimal design for a large set of *n* drive cycles.

Equation (4-7) calculates the driving range, R, for a single combination of E_{batt}, P_{fc}, m_{H2}, and R_{fc}. After an exhaustive search through all viable combinations of these parameters, a matrix of R values is obtained, called R_{matrix}, which is the basis for Fig 5-1 and other similar figures. The dimensions of R_{matrix} are the number of E_{batt} options × the number of P_{fc} options, and a different R_{matrix} is generated for each value of R_{fc} in the exhaustive search. It is proposed that if the design must optimize for n drive cycles, an R_{matrix} should be generated for each cycle, then all resulting matrices should be added together (assuming the matrix dimensions are held constant) to get $R_{matrix,total}$, which is the total range achievable for each design over the n drive cycles, as shown in (5-1). Then, the highest range value from $R_{matrix,total}$ is selected and the corresponding values of E_{batt}, P_{fc}, m_{H2}, and R_{fc} are found to be the optimal design leading to this maximum range over the n cycles.

$$R_{matrix,total} = \sum_{i=1}^{n} R_{matrix,i} \quad \textbf{(5 - 1)}$$

This process is illustrated using the 20 cycles with the highest daily range from the set of real-world logged driving data (the 3 longest cycles are the Cycle 1, 2, and 3 analyzed in prior subsections). The no-refueling case is considered for this example, though the same method can be applied for the refueling case. The daily driving distance of these 20 cycles is summarized in Fig 5-16, and the total distance of these 20 cycles is 8,536.9 km. Table 5-2 shows the top range result for each R_{fc} from 85% to 100%. All four top results have total range within 5.2 km (or 0.07%) of each other, though the bolded row with R_{fc} = 90% gives the highest range of 7,544.9 km with a 30 kWh battery, 19.2 kW fuel cell, and 6.2 kg H_2 tank. The $R_{matrix,total}$ for R_{fc} = 90% is shown in Fig 5-17, where the maximum range is around P_{fc} = 19.2 kW. Thus, the proposed process can be used to find an optimal design for a wide variety of drive cycles.

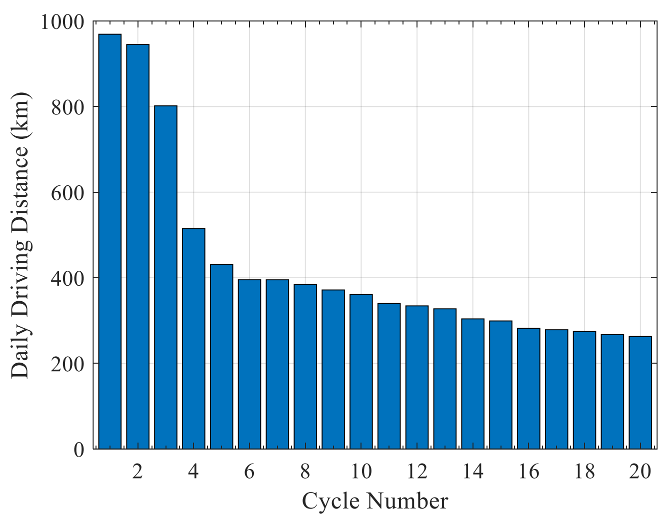

Figure 5- 16: Daily distance of 20 longest real-world drive cycles used for finding a single optimal design

TABLE 5-2: Optimal WDDP-FCREV Design for 20 Real-World Cycles

R_{fc}	Max Range (km)	E_{batt} (kWh)	P_{fc} (kW)	m_{H2} (kg)
100%	7539.7	30	17.4	6.6
95%	7544.4	30	18.3	6.4
90%	**7544.9**	**30**	**19.2**	**6.2**
85%	7542.9	30	20.3	6.0

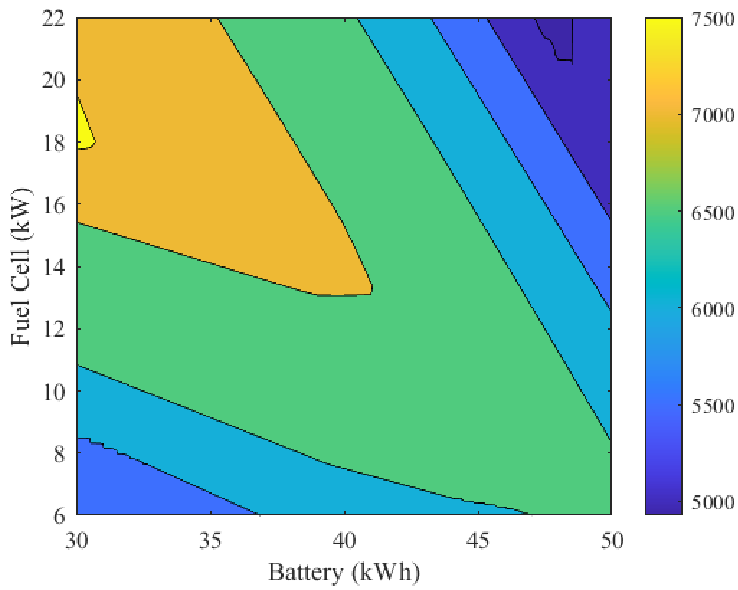

Figure 5- 17: $R_{matrix,total}$ for R_{fc} = 90% for the 20 longest real-world drive cycles

Chapter 6

Conclusions and Future Work

6.1 Summary and Conclusions

This thesis has firstly proposed the concept of the WDDP-FCREV, where the range-extender fuel cell is turned on at the start of a long-distance driving day to maximize the time it can charge the battery, which occurs during driving and parked times. This thesis gives a review of control strategies for FCHVs and FCREVs in Chapter 2. Chapter 2 also compares the differences between applying WDDP control strategy to PHEVs or FCREVs.

In Chapter 3, a Chevrolet Bolt BEV model in MATLAB/Simulink is introduced at a high level and validated through real-world logged drive cycles. The model energy differences compared to real-world measured energy are under 2.31%. The FCREV model is modified based on Chevrolet Bolt model by adding fuel cell system, which contains fuel cell, high-pressure hydrogen tank and dc/dc inverter using a series drivetrain.

In Chapter 4, a fast-analytical design optimization algorithm is proposed and validated to find the optimum combination of fuel cell, battery, and hydrogen tank size, as well as fuel cell operating power, for a selected test drive cycle and a fixed cost. The proposed optimization algorithm speeds up the investigation of the design search space by 20 thousand times, from hundreds of hours to a few seconds, with a very limited impact on accuracy. The fast speed of the algorithm allows the designer to investigate many different test drive cycles, and perform important sensitivity analyses, for example, by varying accessory loads or component costs, since future costs can be uncertain. The proposed fast analytical algorithm is also validated on the customized long-distance drive cycle for both no refueling and refueling cases by comparing battery SOC and driving range with simulated FCREV model in Chapter 4.

Chapter 5 shows the optimization results of the customized drive cycle and real-world drive cycles. For the considered real world drive cycles and component costs, an optimized WDDP-FCREV with the same cost as the Bolt BEV can achieve 105% to 150% longer range than the BEV when H_2 refueling is not considered and 150% to 250% longer range than the BEV when H_2 refueling is allowed every 4 hours from the start of the driving day. These results have important real-world implications for the future design of long-range emission-free passenger vehicles, as these longer ranges are highly desirable for drivers. Alternatively, the energy storage cost of a WDDP-FCREV could be reduced to about 75% of that of a BEV, while achieving the same range as the BEV. Compared to fast-charging BEVs, this thesis shows that WDDP-FCREV has a significant advantage in total drive range when it comes to 5-minute refueling/re-charging. Various optimization studies based on driving range, vehicle cost, drive cycles are investigated in the Chapter 5.

6.2 Suggested Future Work

The proposed optimization algorithm in this thesis is investigated in the passenger vehicle, and it can be extended to other electrified transportation applications, such as taxis and delivery trucks. There are certain long-period routes scheduled for delivery trucks, which can be optimized offline in the algorithm with the lowest energy system cost. The proposed optimization algorithm can be used to design FCREVs in a variety of applications, with variations in drive cycles, component costs, and auxiliary loads.

The WDDP strategy can be further investigated for real-time range prediction to determine the best time to turn on the fuel cell, perhaps somewhat later than the start of the day. Although this adds complexity to the real-time control, an investigation may show whether any potential fuel savings from this concept are significant enough to warrant the extra complexity. Real-time traffic data can be collected and considered to re-compare new estimated energy usage to current usable energy once the routes are changed based on updated traffic information. The original proposed WDDP strategy is simple, robust, and will maximize range on long-distance driving days, which is an important requirement for drivers. However, by expanding the WDDP strategy to update energy use in real-time, hydrogen fuel use could conceivably be reduced.

References

[1] GreenHydrogen. HyProvide A-Series. Accessed: Oct. 20, 2019. [Online]. Available:https://greenhydrogen.dk/wp-content/uploads/2019/11/HyProvideTM-A-Series.pdf

[2] M. A. H. Rafi and J. Bauman, "A Comprehensive Review of DC Fast-Charging Stations With Energy Storage: Architectures, Power Converters, and Analysis," *IEEE Trans. on Transportation Electrification*, vol. 7, no. 2, pp. 345-368, June 2021.

[3] H. Lohse-Busch et. al, “Technology Assessment of a Fuel Cell Vehicle: 2017 Toyota Mirai”, Energy Systems Division, Argonne National Laboratory, Report # ANL/ESD-18/12, June 2018. Available: https://publications.anl.gov/anlpubs/2018/06/144774.pdf.

[4] L. Christensen, J. Klauenberg, O. Kveiborg and C. Rudolph, "Suitability of Commercial Transport for a Shift to Electric Mobility with Denmark and Germany as Use Cases," *Research in Transportation Economics*, vol. 64, 09 2017.

[5] M. Yilmaz and P. T. Krein, "Review of Battery Charger Topologies, Charging Power Levels, and Infrastructure for Plug-In Electric and Hybrid Vehicles," in *IEEE Trans. on Power Electronics*, vol. 28, no. 5, pp. 2151-2169, May 2013.

[6] C. Argue, "What can 6,000 electric vehicles tell us about EV battery health?" GEOTAB, 7 July 2020. [Online]. Available: https://www.geotab.com/blog/ev-battery-health/

[7] M. Keyser, A. Pesaran and Q. Li, "Enabling fast charging – Battery thermal considerations," *Journal of Power Sources*, vol. 367, no. 0378-7753, pp. 228-236, 2017.

[8] S. Samuelsen, "The automotive future belongs to fuel cells range, adaptability, and refueling time will ultimately put hydrogen fuel cells ahead of batteries," in *IEEE Spectrum*, vol. 54, no. 2, pp. 38-43, February 2017.

[9] "TEESING NEWSLETTERS," TEESING, [Online]. Available: https://www.teesing.com/en/page/news-items/sustainable-700-bar-filling-technique-for-furure-hydrogen-cars.

[10] "Hydrogen Storage”, U.S. Office of Energy Efficiency and Renewable Energy [Online]. Available: https://www.energy.gov/eere/fuelcells/ hydrogen-storage.

[11] "Lithium ion Rechargeable battery NCR18650B," Panasonic, 7 October 2016. [Online]. Available: https://www.orbtronic.com/content/ NCR18650B-Datasheet-Panasonic-Specifications.pdf.

[12] Y. Wang, B. Seo, B. Wang, N. Zamel, K. Jiao and X. C. Adroher, "Fundamentals, materials, and machine learning of polymer electrolyte membrane fuel cell technology," *Energy and AI*, vol. 1, no. 2666-5468, p. 100014, 2020.

[13] T. Rudolf, T. Schürmann, S. Schwab and S. Hohmann, "Toward Holistic Energy Management Strategies for Fuel Cell Hybrid Electric Vehicles in Heavy-Duty Applications," in *Proceedings of the IEEE*, vol. 109, no. 6, pp. 1094-1114, June 2021.

[14] "Hyundai Hydrogen Mobility Partnership with H2Energy," Hyundai Hydrogen Mobility AG, 8 July 2020. [Online]. Available: https://hyundai-hm.com/en/2020/07/08/worlds-first-fuel-cell-heavy-duty-truck-hyundai-xcient-fuel-cell-heads-to-europe-for-commercial-use/.

[15] "Nikola Details North American Fuel-Cell Vehicle Program," Nikola, 23 February 2021. [Online]. Available: https://nikolamotor.com/press_releases/nikola-details-north-american-fuel-cell-vehicle-program-112.

[16] K. Kendall, M. Kendall, B. Liang, and Z. Liu, “Hydrogen vehicles in China: Replacing the western model,” *Int. J. Hydrogen Energy*, vol. 42, pp. 30179-30185, 2017.

[17] W. Xiao, Y. Cheng, W. Lee, V. Chen and S. Charoensri, "Hydrogen filling station design for fuel cell vehicles," *2010 IEEE Industrial and Commercial Power Systems Technical Conference - Conference Record*, Tallahassee, FL, USA, 2010, pp. 1-6.

[18] C. I. Hoarcă and F. M. Enescu, "On the energy efficiency of standalone fuel cell/renewable hybrid power sources Part II: Simulation results for variable load profile with different renewable energy sources profiles (RES)," *2018 International Conference on Applied and Theoretical Electricity (ICATE)*, 2018, pp. 1-5.

[19] J. Bauman and M. Kazerani, "An Analytical Optimization Method for Improved Fuel Cell–Battery–Ultracapacitor Powertrain," in *IEEE Transactions on Vehicular Technology*, vol. 58, no. 7, pp. 3186-3197, Sept. 2009.

[20] J. Snoussi, S. B. Elghali, M. Benbouzid and M. F. Mimouni, "Optimal Sizing of Energy Storage Systems Using Frequency-Separation-Based Energy Management for Fuel Cell Hybrid Electric Vehicles," in *IEEE Trans. on Vehicular Technology*, vol. 67, no. 10, pp. 9337-9346, 2018.

[21] Y. Wang, Z. Sun, X. Li, X. Yang, and Z. Chen, ‘‘A comparative study of power allocation strategies used in fuel cell and ultracapacitor hybrid systems,’’ *Energy*, vol. 189, Art. no. 116142, 2019.

[22] Y. Wang, Z. Sun, and Z. Chen, ‘‘Energy management strategy for battery/supercapacitor/fuel cell hybrid source vehicles based on finite state machine,’’ *Appl. Energy*, vol. 254, Art. No. 113707, 2019.

[23] H. Li, A. Ravey, A. N'Diaye, and A. Djerdir, ''A novel equivalent consumption minimization strategy for hybrid electric vehicle powered by fuel cell, battery and supercapacitor,'' *Journal of Power Sources*, vol. 395, pp. 262-270, 2018.

[24] N. Sulaiman, M. A. Hannan, A. Mohamed, P. J. Ker, E. H. Majlan, and W. R. Wan Daud, "Optimization of energy management system for fuel-cell hybrid electric vehicles: Issues and recommendations," *Appl. Energy*, vol. 228, pp. 2061-2079, 2018.

[25] J. Li, H. Wang, H. He, Z. Wei, Q. Yang and P. Igic, "Battery optimal sizing under a synergistic framework with DQN based power managements for the fuel cell hybrid powertrain," *IEEE Trans. on Transportation Electrification*, Early Access Article, 2021.

[26] X. Chi, F. Lin and Y. -X. Wang, "Disturbance and uncertainty-immune onboard charging batteries with fuel cell by using equivalent load fuzzy logic estimation-based backstepping sliding-mode control," in *IEEE Trans. on Transportation Electrification*, vol. 7, no. 3, pp. 1249-1259, 2021.

[27] J. Chen, C. Xu, C. Wu, and W. Xu, "Adaptive fuzzy logic control of fuel-cell-battery hybrid systems for electric vehicles," *IEEE Trans. Industrial Informatics*, vol. 14, no. 1, pp. 292–300, 2018.

[28] F. Tao, L. Zhu, Z. Fu, P. Si, L. Sun, "Frequency decoupling-based energy management strategy for fuel cell/battery/ultracapacitor hybrid vehicle using fuzzy control method," *IEEE Access*, vol. 8, pp. 166491-166502, 2020.

[29] R. Á. Fernández, S. C. Caraballo, F. B. Cilleruelo and J. A. L. Lozano, "Fuel optimization strategy for hydrogen fuel cell range extender vehicles applying genetic algorithms," *Renewable and Sustainable Energy Reviews*, vol. 81, pp. 655-668, 2018.

[30] B. Geng, J. K. Mills and D. Sun, "Two-stage energy management control of fuel cell plug-in hybrid electric vehicles considering fuel cell longevity," in *IEEE Trans. on Vehicular Technology*, vol. 61, no. 2, pp. 498-508, Feb. 2012.

[31] Y. Zhang, C. Zhang, Z. Huang, L. Xu, Z. Liu and M. Liu, "Real-time energy management strategy for fuel cell range extender vehicles based on nonlinear control," in *IEEE Trans. on Transportation Electrification*, vol. 5, no. 4, pp. 1294-1305, Dec. 2019.

[32] Y. Liu, J. Li, Z. Chen, D. Qin, and Y. Zhang, "Research on a multiobjective hierarchical prediction energy management strategy for range extended fuel cell vehicles," *J. Power Sources*, vol. 429, pp. 55-66, 2019.

[33] S. Molina, R. Novella, B. Pla, M. Lopez-Juarez, "Optimization and sizing of a fuel cell range extender vehicle for passenger car applications in driving cycle conditions," *Applied Energy*, vol. 285(C), 2021.

[34] X. Wu, X. Hu, X. Yin, L. Li, Z. Zeng, V. Pickert, Convex programming energy management and components sizing of a plug-in fuel cell urban logistics vehicle, *J. Power Sources*, vol. 423, pp. 358-366, 2019.

[35] P. Palcu and J. Bauman, "Whole-day driving prediction control strategy: analysis on real-world drive cycles," in *IEEE Trans. on Transportation Electrification*, vol. 4, no. 1, pp. 172-183, March 2018.

[36] P. Pei, Q. Chang, T. Tang, "A quick evaluating method for automotive fuel cell lifetime," *International Journal of Hydrogen Energy*, vol. 33, pp. 3829-3836, 2008.

[37] "CHEVROLET BOLT EV - 2017," CHEVROLET, 2017. [Online]. Available: https://media.gm.com/media/us/en/chevrolet/vehicles/bolt-ev/2017.tab1.html.

[38] "GM's Korea studio 'broke the mold' with Bolt". A.News. August 3, 2016. [Online]. https://www.autonews.com/article/20160807/OEM03/160809904/gm-s-korea-studio-broke-the-mold-with-bolt.

[39] Argonne National Lab Autonomie, Vehicle Modeling Software [Online]. https://www.anl.gov/partnerships/autonomie-automotive-system-design.

[40] "BDC546 - Bidirectional 750 V DC/DC-Converter," BRUSA, March 2021. [Online]. Available: https://www.brusa.biz/wp-content/uploads/2021/03/BRUSA_Factsheet_BDC546.pdf.

[41] "Toyota Mirai FCV Posters LR Tcm-11-564265," Toyota Motor Europe, [Online].Available:https://www.toyotaeurope.com/download/cms/euen/Toyota%20Mirai%20FCV_Posters_LR_tcm-11-564265.pdf.

[42] H. Yumiya, M. Kizaki and H. Asai, "Toyota Fuel Cell System (TFCS)," *World Electric Vehicle Journal*, vol. 7, pp. 85-92, March 2015.

[43] H. Marzougui, A. Kadri, M. Amari and F. Bacha, "Energy Management of Fuel Cell Vehicle with Hybrid Storage System: A Frequency Based Distribution," *2019 6th International Conference on Control, Decision and Information Technologies (CoDIT)*, 2019, pp. 1853-1858.

[44] W. Schmid, L. Wildfeuer, J. Kreibich, R. Büechl, M. Schuller and M. Lienkamp, "A Longitudinal Simulation Model for a Fuel Cell Hybrid Vehicle: Experimental Parameterization and Validation with a Production Car," *2019 Fourteenth International Conference on Ecological Vehicles and Renewable Energies (EVER)*, 2019, pp. 1-13.

[45] M. E. Aydin and T. C. Fogarty, "A distributed evolutionary simulated annealing algorithm for combinatorial optimisation problems," *Journal of heuristics*, vol. 10, pp. 269-292, 2004.

[46] N. Leahey and J. Bauman, "A Fast Plant-Controller Optimization Process for Mild Hybrid Vehicles," in *IEEE Trans. on Transportation Electrification*, vol. 5, no. 2, pp. 444-455, June 2019.

[47] V. Henze, "Battery Pack Prices Fall As Market Ramps Up With Market Average At $156/kWh In 2019," Bloomberg NEF, 3 December 2019. [Online]. Available: https://about.bnef.com/blog/battery-pack-prices-fall-as-market-ramps-up-with-market-average-at-156-kwh-in-2019/.

[48] A. Wilson, G. Kleen and D. Papageorgopoulos, "Fuel Cell System Cost - 2017," DOE, September 2017. [Online]. Available: https://www.hydrogen.energy.gov/pdfs/17007_fuel_cell_system_cost_2017.pdf.

[49] "US DRIVE Electrical and Electronics Technical Team Roadmap," ENERGY.GOV, 29 July 2013. [Online]. Available: https://www.energy.gov/sites/default/files/2017/11/f39/EETT%20Roadmap%20 10-27-17.pdf.

[50] J. Adams, C. Houchins and R. Ahluwalia, "Onboard Type IV Compressed Hydrogen Storage System -," DOE, 25 Novermber 2019. [Online]. Available:https://www.hydrogen.energy.gov/pdfs/19008_onboard_storage _cost_performance_status.pdf.

[51] M. Mueller, “5 Things to Know When Filling Up Your Fuel Cell Electric Vehicle,” U.S. Department of Energy, Office of Energy Efficiency and Renewable Energy, July 2016. [Online]. Available: https://www.energy.gov/eere/articles/5-things-know-when-filling-your-fuel-cell-electric-vehicle.